Development and Characterization of PMMA Based Porous Materials Used for High Pressure Casting of Sanitaryware Ceramics

By

Yelda ERGÜN

**A Dissertation Submitted to the
Graduate School in Partial Fulfillment of the
Requirements for the Degree of**

MASTER OF SCIENCE

**Department: Materials Science and Engineering
Major: Materials Science and Engineering**

**Izmir Institute of Technology
Izmir, Turkey**

July, 2004

We approve the thesis of Yelda ERGÜN Date of Signature

Assoc.Prof.Dr. Metin TANOĞLU
Supervisor
Department of Mechanical Engineering

Prof.Dr. Muhsin ÇİFTÇİOĞLU
Co-Supervisor
Head of Interdisciplinary Material Science
and Engineering Programme

Assoc.Prof.Dr. Mustafa GÜDEN

Department of Mechanical Engineering

Assoc.Prof.Dr. Sacide ALSOY
Department of Chemical Engineering

Assoc.Prof.Dr. Sedat AKKURT

Department of Mechanical Engineering

ACKNOWLEDGEMENTS

I would like to acknowledge the people who have helped to make this work possible. My sincere gratitude is first for my thesis advisor Assoc.Prof. Metin Tanoğlu for his consistent and thoughtful advice, continuous encouragement and help during this study. I would like to thank to Prof.Dr. Muhsin Çiftçioğlu for his valuable comments and recommendations.

I acknowledge Ege Vitrifiye Sanitaryware Inc. of Turkey for the financial support and I wish to specially thank to C. Tokman, C. Dirier, M. Yılmaz and E. Erdoğan of Ege Vitrifiye Sanitaryware Inc. for their valuable help during my studies. I also wish to thank to personnel of IZTECH Centre for Material Research for their help during my material characterization studies.

I am grateful to my friends for assisting me with my research and offering advice and discussion. Specifically I would like to thank Mehmet Şahin, Emre Kuduğ and Beyhan Cansever.

Finally, I would like to express my heartfelt gratitude to my parents for their continuous support and encouragement, which enabled me to overcome difficulties.

ABSTRACT

The ceramic whiteware / sanitaryware industry is rapidly undergoing to implement high-pressure casting techniques for ceramic article production. In high pressure technique, porous materials with open cell microstructure that allow drainage of water from the ceramic suspension under applied pressure are needed. In addition, a relatively high mechanical performance of the porous structure is required to obtain a long service life from the material under the cycled high pressures. The polymethyl methacrylate (PMMA) based polymeric porous structures have become the most suitable type of materials for this purpose because of their short casting periods and high service lives. The superior service life and performance of these materials are closely related to their microstructure.

In the present study, PMMA-based porous materials were produced by water-in-oil emulsion polymerization technique. The porous systems were produced with various compositions of the constituents in the emulsion and various filler sizes to investigate the effect of the constituents and the sizes on the microstructure of PMMA-based materials. The variations on the pore microstructure were related to the performance of the material. The pore morphology and porosity of the samples was investigated using optical and scanning electron microscopy techniques (SEM). Water permeability was measured using a custom made permeability apparatus. The mechanical properties such as compressive collapse stress and elastic modulus values were determined by performing mechanical compression tests. It was found that increasing water surfactant concentration increases the porosity, water permeability and decreases mechanical properties and reversely increasing the amount of monomer in the emulsion decreases the porosity, water permeability and increases the mechanical properties. Fracture toughness values of the materials were measured by using single edge notch three point bending (SENB) test method. Fracture toughness test results and fracture surface analysis show that materials are fractured in brittle manner. It was found that lower concentrations of water and higher concentrations of monomer result in thicker cell walls and improve the fracture toughness of the material. To investigate the residual mechanical properties, specimens were subjected to cyclic loadings. After cyclic loading, increase of elastic modulus with the percentage of 52 and decrease of collapse stress values were measured.

ÖZET

Seramik endüstrisi, seramik ürün elde edebilmek için hızla yüksek basınçlı döküm tekniğini kullanmaya başlamıştır. Yüksek basınçlı kalıplama tekniğinde mekanik olarak dayanıklı, açık-hücre gözeneklere sahip ve uygulanan basınç altında su geçirgenliğine imkan veren malzemelere gerek duyulmaktadır. Bununla birlikte, gözenekli yapının uygulanan periyodik yüksek basınçlar altında uzun ömürlü olabilmesi için daha yüksek mekanik performansa sahip olması gerekmektedir. PMMA esaslı polimerik malzemeler kısa döküm periyotları ve uzun kullanım süreleri dolayısıyla en uygun malzemeler haline gelmişlerdir. Bu malzemelerin uzun kullanım süreleri ve performansları malzemenin mikro-yapısıyla yakından ilgilidir. Bu çalışmada PMMA esaslı açık-hücre gözenekli plastik malzemeler yağ içinde su emülsiyonunun polimerizasyonu tekniği ile üretilmiştir. PMMA esaslı malzemelerin mikro-yapısı üzerindeki etkisini incelemek üzere emülsiyon bileşenlerinin çeşitli oranları ve çeşitli tane boyutlarda dolgu malzemeleri kullanılarak gözenekli malzemeler üretilmiştir. Gözenek yapısındaki değişim malzemenin performansı ile ilişkilendirilmiştir Numunelerin gözenek yapısı ve gözeneklilik oranları optik ve taramalı elektron mikroskobu kullanılarak incelenmiştir. Su geçirgenliği özel tasarlanan bir geçirgenlik aparatı kullanılarak ölçülmüştür. Malzemenin çökme stresi ve elastik modül gibi mekanik özellikleri basma testleri düzenlenerek belirlenmiştir. Su ve surfactant miktarının arttırılması malzemelerin gözeneklilik oranını, su geçirgenliğini arttırmış mekanik dayanımını azaltmıştır. Bununla birlikte monomer miktarının arttırılması gözeneklilik oranını, su geçirgenliğini azaltmış ve mekanik dayanımını arttırmıştır. Malzemelerin kırılma tokluğu değerleri çentikli üç nokta eğme test metodu kullanılarak ölçülmüştür. Test sonuçları ve kırılma yüzeyi görüntüleri malzemelerin gevreksi kırıldığını göstermiştir. Düşük su-surfactant ve yüksek monomer konsantrasyonu kalın hücre duvarlarının oluşumunu sağlamaktadır bu da malzemenin kırılma tokluğunu arttırmıştır. Kalan mekanik özelliklerinin saptanabilmesi için numuneler periyodik yükleme testlerine tabi tutulmuştur. Periyodik yüklemenin ardından malzemelerin elastik modül değerinin 52% oranında arttığı ve çökme stresi değerinin azaldığı ölçülmüştür.

TABLE OF CONTENTS

LIST OF FIGURES

LIST OF TABLES

Chapter 1
INTRODUCTION

Plastic materials have many advantages when compared with metallic and ceramic materials due to their easy production, shaping and applicability. They became preferable in many processes such as, in production of ceramic whiteware and sanitaryware articles with slip casting technique. Porous plastic mold materials have been replaced with the traditional plaster molds due to their improved properties.

Traditionally, slip casting process for the shaping of ceramic sanitaryware and whiteware articles has been performed by using plaster molds. This material contains an open cell structure with a mean pore size of about 1 μm and it operates under the principle of capillarity and absorbs water from the ceramic slip. Plaster molds are inexpensive, suitable for machining and operate without external pressure. However, they exhibit long casting periods (1-2 hours), long drying time and have limited service life due to their low wear resistance (80-100 maximum cast). Moreover, cast part contains high amount of water that has to be removed by drying with some additional cost.

To overcome the limitations of the plaster of Paris and improve the ceramic article quality and productivity, the trend in the ceramic industry is the utilization of the high pressure casting process that provides automation. In this technique, a porous mold material that allows the drainage of water from the slip under high pressures of typically 13-15 bars is needed [1]. The materials with an open cell structure need to provide high water permeability, high mechanical strength and fatigue performance. These materials are also expected to keep the integrity of the structure without deformation and allow the usage of high pressures to provide a tight seal around the mold without cracking along about 20,000 cycles during expected service life.

Polymeric materials, especially PMMA-based porous materials, became the most suitable one for this purpose. Using these type of materials, casting and demolding period can be shortened up to 20 min., molds require no drying between the casting cycles since air-purging system is used for dewatering and therefore mold can be returned to the service immediately. Furthermore, casting period can be adjusted by changing the slip pressure within the limits of the mechanical strength of the mold material. However, it needs special attention that the service life and performance of

plastic mold is closely related to the microstructure and mechanical properties of the material. Therefore, fundamental understanding of the processing, microstructure and property relationship in these materials is essential to obtain optimized performance. To our knowledge, there is very limited work reported in the literature about the subject. In recent studies, Pique et. al. studied measurement of the fracture toughness of PMMA-based porous plastic molds and they used fictitious crack model for modeling the fracture behavior [2]. In addition, the same group has studies on improvement of the mechanical performance of these materials by addition of reinforcing components such as clay particles into the plastic structure [3, 4].

In this study, plastic materials with various pore morphologies were produced by polymerization of water-in-oil emulsions with various compositions of the emulsion constituents and particle sizes of the PMMA based filler beads. The effects of changing the compositions and bead sizes on the pore fraction and morphologies were investigated by SEM and optical microscopy techniques. Also, the relation between the morphology, water permeability and mechanical properties of the porous materials was investigated. Measurement of water permeability was done by using a custom made permeability apparatus. Compressive mechanical testing was performed to obtain the stress-strain behavior, elastic modulus and collapse stresses and to investigate the deformation mechanisms of the materials. In the literature, there are some recent studies related to the prediction of the dependence of mechanical properties on the density of the cellular materials. Ashby and Gibson used a simple cubic model for periodic, low density cellular materials to predict their dependence of strength and elastic modulus on density [5]. The difference between model and experimental data for the randomly distributed or high density cellular materials showed that the theory of Ashby and Gibson should be revised for these materials. Roberts and Garboczi have simulated random cellular materials with wide density ranges by using finite element analysis (FEA) and developed an analytical equation [6]. Predictions of these two theories were compared for PMMA based porous materials developed within this study. Fracture toughness values of the materials were measured based on single edge notch bending (SENB) test and fracture surfaces were investigated by using SEM to understand the fracture mechanisms. Deformation of these materials under cycled loading is critical for their molding applications. For the investigation of the residual mechanical properties and deformation mechanisms after cyclic loading, specimens were subjected to 1000 cycle loading and then static loadings were performed on the same specimens up to

fracture point. It is also known that the contribution of inorganic materials to organic structures frequently exhibit unexpected improved mechanical properties such as in PMMA based emulsion systems [4, 7]. To investigate the effect of additional inorganic reinforcement materials, nanoscale layered clay particles (montmorillonite) was added to emulsion with and without organical modify cation.

Chapter 2

PRODUCTION OF SANITARYWARE CERAMICS BY SLIP CASTING

Production techniques of traditional ceramics (clay-based ceramics) can be grouped under three basic headings; dry pressing, plastic forming, and slip casting. Slip casting is a method for powder based shaping of ceramic articles and has some advantages, including availability to produce geometrically complex shape articles with very good material homogeneity due to the slurry properties, such as sanitarywares. It is a filtration process, in which a powder suspension, usually water based suspension, is poured into porous mold. Two types of slip casting techniques are used for the shaping; conventional and pressure slip casting. Most of the ceramic goods are still shaped by conventional slip casting technique employing plaster molds today, but development trend is towards high pressure casting with porous polymeric molds [8]. Fig. 2.1. is a schematic illustration of the casting process and water transport in these techniques which will be described in detail below.

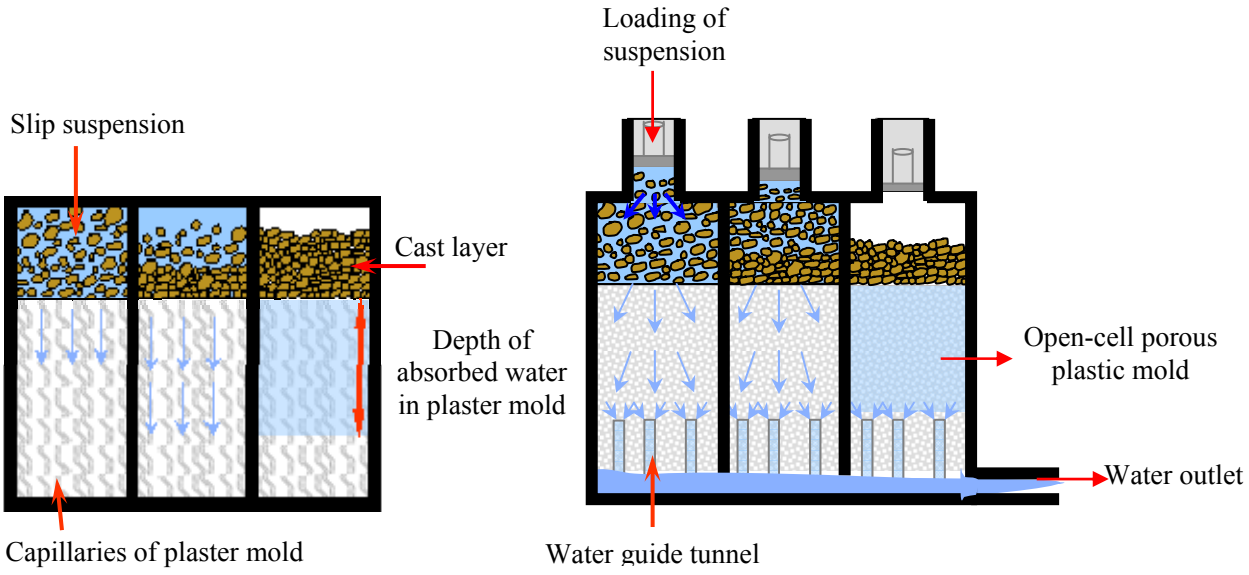

Figure. 2.1. Illustration of slip casting techniques, a) casting with plaster mold, b) high pressure casting

2.1. Preparation of Raw Materials and Properties of Casting Slip

Raw materials used for the production of sanitaryware ceramics are kaolin, quartz, feldspar and some dispersion additives. A typical batch consists of approximately 40 to 50 % kaolin (Al_2O_3 .$2SiO_2$. $2H_2O$), 20 to 30 % quartz (SiO_2), 20 to 30 % feldspar (R_2O. Al_2O_3. $6SiO_2$) and very low percentage of dispersion additives. Fig. 2.2 shows the crystal structures of kaolin and quartz. To prepare the raw materials for wet processes, they are suspended in water, crushed and ground until the particle diameter is reduced. Then, suspension is screened to remove the impurities and following this step it is homogenized in stirred tanks. The particles in the casting slip tend to agglomerate, which is called as flocculation. To prevent flocculation, a variety of chemicals and electrolytes are used to break up these agglomerates. Common deflocculants used in slips containing clays are sodium silicate, sodium carbonate, sodium phosphate and some organic substances such as polyacrylates [9].

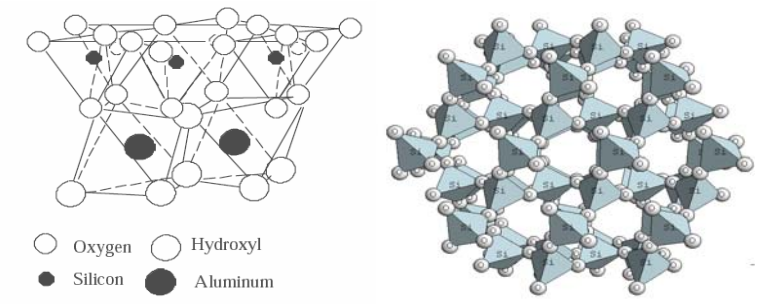

(a) (b)

Figure 2.2. Crystal structures of a) kaolin and b) quartz [10].

Control of the casting slip is critical and there are a number of slip properties that are desirable for an optimum process. The casting behavior of ceramic slips depends strongly on slip`s specific gravity, viscosity and change in viscosity with respect to time. The viscosity of the slip is a function of the mean particle diameter, content and the nature of the solids present. Slip should have low viscosity to allow all parts of the mold to be easily filled and to prevent trapping of air bubbles. The specific gravity is a simple measurement of the amount of solid suspended in slip. Specific gravity of the slip should be high enough to shorten casting time, lower the amount of

water that must be processed and also increase green density. Cast piece should also have low drying shrinkage, easy mold release, adequate green strength in the cast layer to allow easier handling. With regard to raw materials, kaolin influences the rheology more than feldspar and quartz. In pressure casting, kaolin controls the casting rate and percentage of kaolin is kept higher in pressure casting slips. The permeability of the pressure casting slip is usually higher than the conventional slip [11].

2.2. Traditional Slip Casting

Production of ceramic articles by using plaster molds, called as conventional slip casting, has been introduced on a commercial scale as early as the 18^{th} (1740) century in England for the production of tableware pieces. Slip casting by using plaster molds has been used for the production of sanitaryware since the invention of flushing toilets at the end of the 19^{th} century [12].

2.2.1. Plaster Molds for Traditional Slip Casting

Plaster is made of calcium sulfate hemihydrates $CaSO_4.0.5H_2O$. Hemihydrates is not present in nature, but can be obtained from widely distributed natural products such as calcium sulfate dihydrate (gypsum rock), $CaSO_4.2H_2O$. This natural product contains some impurities such as clay, chalk, dolomite, silica and metallic oxides. The name plaster of Paris usually refers to the calcium sulfate hemihydrates obtained from the purest parts of the natural products and used for molding applications. To produce hemihydrates from dihydrate, gypsum rock is calcined in order to remove part of the crystal water from calcium sulfate crystals and then it is ground to obtain a powder with a suitable particle size distribution. When using plaster as mold material, it has to be prepared in the form of slurry with water and some additives to modify the properties according to customer requirements. By mixing the plaster with water, hemihydrates structure becomes dihydrated.

$$CaSO_4 . 0.5H_2O + 1.5\ H_2O \longrightarrow CaSO_4 . 2H_2O$$

Excess water in the slurry is eliminated by drying process and the spaces filled with water generate the porous structure of the hardened plaster mold. During the settling of the material, interconnecting network of needle and plate-like arrangements

Figure 2.3. SEM micrograph of plaster mold [13].

of gypsum crystals is formed as illustrated in Fig 2.3 and this arrangement gives strength to the mold. In sanitaryware industry, from 68 to 90 parts by weight of water to 100 parts plaster is used [9]. Mold produced with higher plaster ratio has higher mechanical strength, lower porosity and higher expansion.

Plaster molds operate on the principle of capillarity as shown in Fig.2.1. Water is absorbed by the mold at its surface and removed from the slip. As a result, a layer of material is formed with low water content which will be self-supporting when the mold is removed. After a layer of proper thickness has formed, the remaining slip is drained from the mold. The formed part is allowed to remain in the mold for additional water removal by mold absorption and evaporation, until the part has become physically strong enough to support itself. The mold is taken apart to release the part and it is left to dry as illustrated in Fig.2.4.

Plaster mold is easily shaped, operate without pressure and relatively inexpensive as it is produced from natural resources. But, it has several drawbacks. Casting and drying time of the mold is very long, only one or two casting is available per a day and also the molds typically have a limited working life, they become useless after about one hundred castings because of the low resistance to wear [14]. All these make plaster molds impractical for industrial large-volume operations.

Figure 2.4. Production by plaster mold [15].

2.3. Pressure Casting

Pressure slip casting is basically similar to the traditional slip casting; however, a pressure is applied to the slip to force water from the slip through the mold. As illustrated in Fig.2.1 driving force in the mold for removing the water is pressure of 10-15 bars applied in this process, in contrast to slip casting in which capillary suction of the plaster is the mechanism. Pressure casting is being applied in the sanitaryware industry in relatively recent years and provides a number of advantages. Casting times are significantly reduced and parts can be easily demolded. Molds require no drying between casting cycles and thus can be returned to service immediately. Backwashing is applied for removing the slip particles from the mold pores and an air purging system is used to dewater molds. Mold life is much longer than conventional plaster molds and fewer defects occur due to good mold wear resistance. Product quality is more consistent and the cast part has less moisture to remove. This eases drying requirements and reduces drying defects and losses. Parts with variable thickness are easier to mold. One person can operate two or three casting machines and the operation can be run two or three shifts per day.

2.3.1. Plastic Molds for High Pressure Casting

Pressure casting requires special molds with high strength that can withstand the applied pressure. Plaster molds can not withstand the applied pressures, therefore special plastic materials have been developed for this purpose. These materials must have optimized porosity, water permeability, mechanical strength and elasticity. The latter property is required to allow mechanical pressure to be used to provide a very tight seal around the molds without mold cracking.

Plastic (resin) porous mold materials have been used instead of plaster of Paris without any limitation of the complexity of the ceramic articles. Some examples of resin systems that can be used for the production of the plastic molds are epoxy resins, acrylic resins and unsaturated polyester [16-18]. Plastic molds have porosity consisting of larger pores that do not give the same capillary forces and require an externally applied pressure to drive the filtration process; they are commonly used under 13-15-bar of pressure. High-pressure leads to the removal of nearly all fluid content of the pieces and demolding can be done immediately, so a new casting cycle can be started. Casting

period can be adjusted by changing the slip casting pressure in the limitations of the mechanical strength of the molds. This technique significantly reduces labour requirements, however, because of the high pressure and complexity of the automatically controlled production cycles, it needs design of new machines and this requires a considerable economic investment. Hence, their use is only meaningful where the number of output is particularly high and not too much mix product is demanded. In that case, the technique lowers the overall production costs. Fig 2.5 is an example showing the automatic high pressure casting machines.

Figure 2.5. Automatic high pressure casting machines [15].

Chapter 3
EMULSION SYSTEMS

PMMA based porous materials and PMMA beads that were used in this study were produced by emulsion and suspension polymerization techniques, respectively. Suspension and emulsion polymerizations are essentially called as heterogeneous polymerization systems due to the content of non-solvent liquid, usually water, immiscible liquid monomer and surfactant. Fig.3.1 illustrates the types of emulsion systems that are formed by polar and apolar systems. These systems are also called as water-oil systems because water (polar) and monomer (apolar) phases have tendency to separate from each other as water and oil phases. For the homogenous distribution of one phase in the other, surfactants are used. Hydrophobic and hydrophilic ends of the surfactant molecules catch the monomer and water molecules, respectively, and provide the formation of homogeneous emulsion.

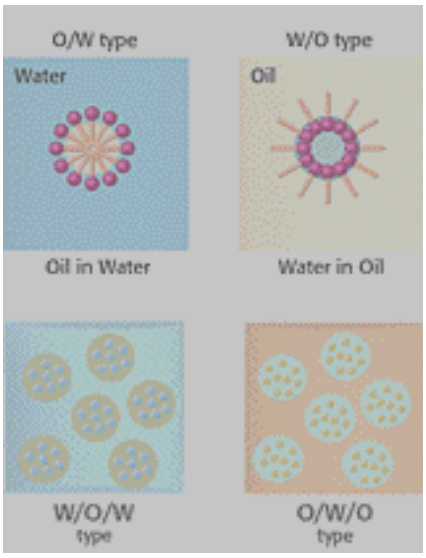

Figure 3.1. Types of Emulsions

3.1. Production of PMMA Beads by Suspension Polymerization

Polymeric beads are commonly produced by oil in water suspension polymerization technique. Suspension polymerization was first developed by Hoffman and Delbruch in 1909 [19] and it was first used for the production of acrylic beads by Bauer and Lauth`s in 1931 [20]. Suspension polymerization technique involves

dispersion of the liquid monomer mass into separate small droplets in a large continuous mass of a nonsolvent, commonly called as dispersion or suspension medium, by efficient agitation or using dispersant. Water is invariably used as the suspension medium for all water insoluble monomers because of many advantages, such as low cost and non-toxic nature. Water (polar) and monomer (apolar) phases have tendency to separate from each other as in water and oil phases. Water forms the continuous phase and monomer phase is distributed in water by using the suitable surfactants (water in oil). Since polymerization occurs within the monomer droplets, the use of an oil-soluble initiator, such as benzoyl peroxide (BPO), azobisisobutyronitrile (AIBN), is required. [21]. Suspension polymerization reactions for the production of polymer beads were initiated using some other ways, such as ultrasound sources [22]. Each small polymerizing droplet in the continuous phase behaves as an isolated batch polymerization reactor. Particle sizes of the produced beads depend on the distribution of monomer phase in the emulsion and activation of the surfactant.

3.2. Emulsion Polymerization

During the production of PMMA based plastic porous materials, within this study final mixture consisted of an immiscible water phase dispersed in the monomer phase and additionally PMMA beads were suspended in the emulsion. This system is called as water in oil emulsion system. Homogeneity and stability of this system is provided by surface active agents (surfactant). Surfactant molecules are classified as ionic or non-ionic depending on whether the head group has a net charge or not. The ionic surfactants are further classified as cationic or anionic depending on whether the head group is positively or negatively charged. PEO-PPO block copolymers are examples of non-ionic surfactants. Non-ionic surfactants are neutral. The head consists of a small molecular group is the hydrophilic and the long polymer chain is the hydrophobic part of the nonionic surfactant molecule [23]. In addition to diblock (PEO-PPO), triblock (PEO-PPO-PEO) copolymers are the other examples of non-ionic surfactants. There is another class of surfactants, called zwitterionic surfactants, which has both of an anion and a cation.

Fig.3.2 shows an illustration of the water in oil emulsion system that was used to produce PMMA based porous materials. Hydrophobic and hydrophilic ends of the PEO-PPO based surfactant catch monomer and water molecules and hold them together,

provide the distribution between the phases. So, the amount of the surface-active agent determines the level of the dispersion. Dispersion level of the emulsion is critical for the diameter, shape and distribution of the pores. A high dispersion level may yield homogeneous distribution of pores with a smaller diameter in the final part. Therefore, dispersion level is critical to obtain the porous structure with optimum properties.

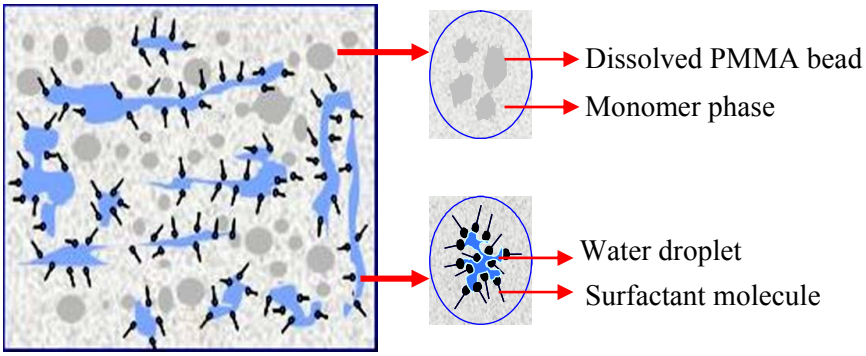

Figure 3.2. Illustration of emulsion system.

3.3. Free Radical Polymerization in the Emulsion

In the emulsion polymerization of PMMA system, free radical polymerization reaction takes place by the effect of initiator (BPO) with the contribution of PMMA beads. Free radical polymerization occurs in three steps; initiation of the reaction with formation of the first radicals, propagation of the polymerization and termination of the radicals. This polymerization process starts with the activation of BPO molecules; they have an ability to fall apart and the pair of electrons in the broken bond separate. Free active electron try to become stable and double bond between the carbon and oxygen atoms is broken by the effect of it to form CO_2 and radical phenyl molecules (Fig.3.3).

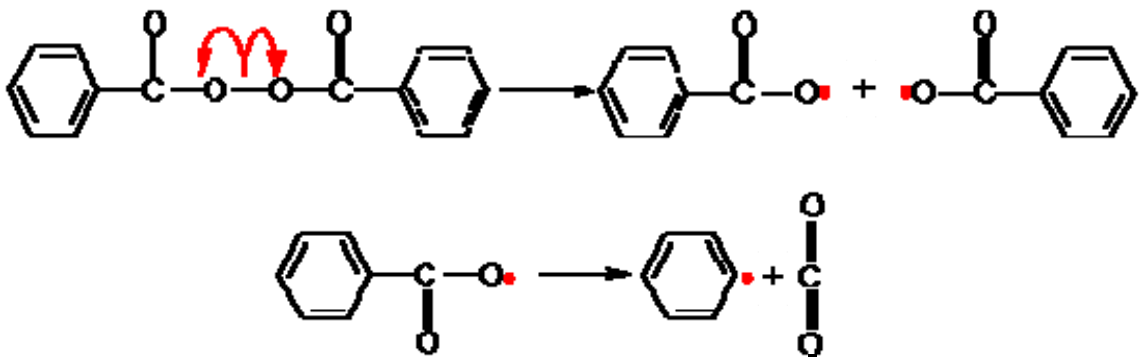

Figure 3.3. Activation of BPO molecules.

The unpaired electron on the phenyl molecule wants to be paired. The carbon-carbon double bond in a methyl methacrylate monomer has a pair of electrons bonded with weaker forces and when the unpaired electron comes near and swipe one of them to pair with it. This new pair of electrons forms a new chemical bond between the initiator phenyl and carbon atom of the monomer molecule. The other electron which is not bonded to the initiator forms a new free radical (Fig.3.4).

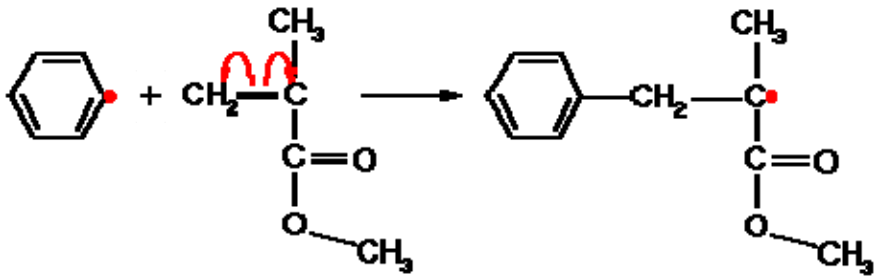

Figure 3.4. Formation of active radical monomer molecule.

Created active MMA molecule has a strong affinity to react with other monomer molecule in the same way as the initiator phenyl molecule did. This reaction takes place over and over again, polymerization reaction is propagated and more monomer molecules join to the growing chains (Fig.3.5)

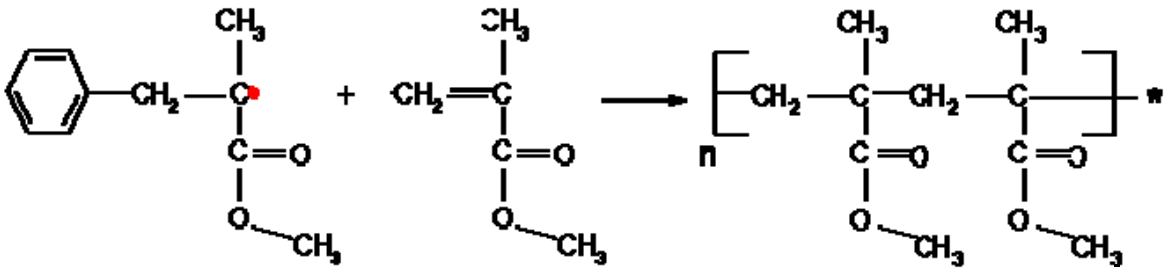

Figure 3.5. Propagation of the polymerization reaction.

Termination of the polymer chain can occur in one of three ways. The active molecule can react with the initiator or with some other impurity that bonds and has no more open sites for continued bonding. Two active molecules can bond together. Or, two active sites can come into contact with one and gives up an atom (usually hydrogen) to the other, so terminating both chains without combining.

Free radical polymerization is an exothermic reaction; released heat and reaction time depends on the amount of the material that will be produced. After polymerization

of the emulsion completed, water molecules find a way and they are removed from the final product and spaces filled with water droplets in the monomer phase form the pores of the materials. With the contribution of the PMMA beads and polymerization of the monomer molecules rigid cell walls are formed.

Chapter 4
CELLULAR (POROUS) MATERIALS

4.1. Microstructure of Cellular Materials

Many materials have cellular structure in nature such as cork, wood, sponge and trabecular bone (Fig.4.1). Natural cellular materials have been taken as model and engineered honeycombs and synthetic cellular materials are fabricated based on polymers, metals, ceramics and glasses (Fig.4.2). Properties and performance of the cellular materials are related to the material from which they are made, geometrical structure of the cells, and the density of the final material. The most important structural characteristic of a cellular solid is its relative density, ρ^*/ρ_s (the ratio of the density of the foam, ρ^*, and the cell wall material bulk density, ρ_s). Microstructural properties of the manufactured cellular materials give them unique properties and they are used in a variety of applications such as thermal insulation [24], energy-absorption devices [25-26], light weight reinforcement, filter material, biomedical applications [27-28], etc. Cellular materials are classified as open-cell and closed-cell. In closed-cell materials, each cell is completely enclosed by thin cell walls, whereas in open-cell materials the individual cells are interconnected. Cellular materials can also be categorized as periodic (Fig.4.2 a) or random cellular materials (Fig.4.2 b) based on the order of the cells.

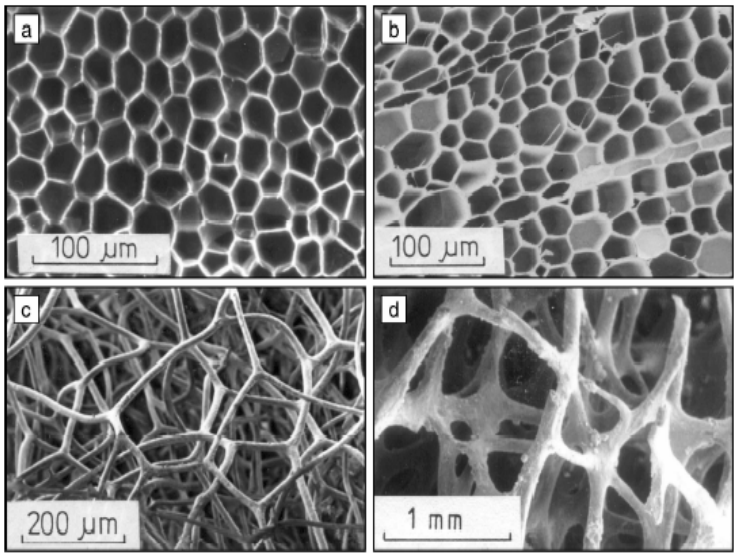

Figure 4.1. Natural cellular materials a) cork, b) wood, c) sponge and d) trabecular bone [5].

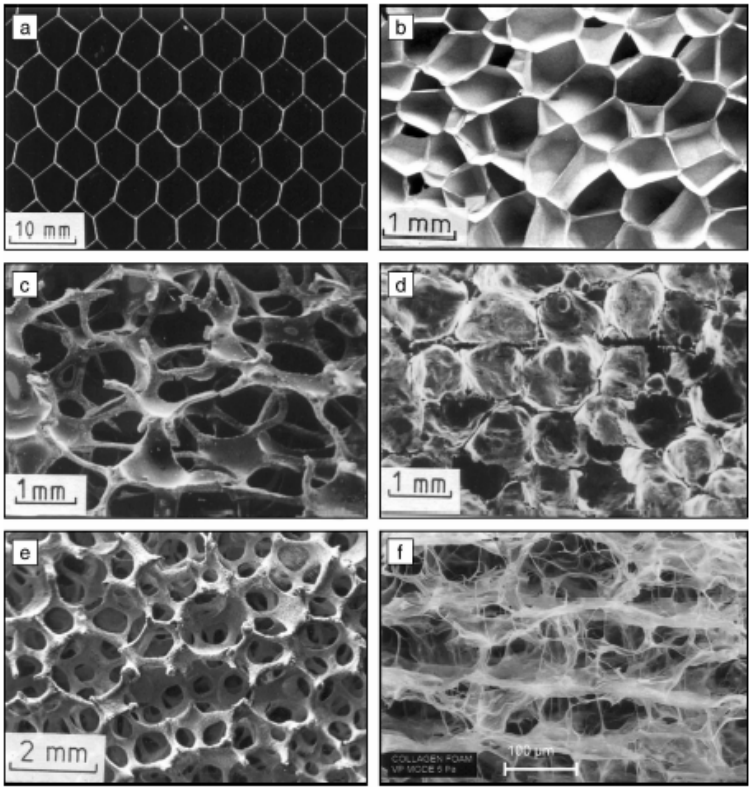

Figure 4.2. Manufactured cellular materials a) aluminum honeycomb, b) closed-cell polyethylene foam, c) open-cell nickel foam, d) closed-cell glass foam, e) open-cell zirconia foam and f) collagen-based scaffold used in tissue engineering [5].

4.2. Mechanical Behavior of Cellular Materials

The mechanical behavior of a cellular solid is related to the geometrical structure of the cells and the densities of the raw and final material. Fig. 4.3 a, b and c show the representative compressive stress-strain curves of elastomeric, elastic-plastic and brittle foam, respectively [5]. They show linear elasticity at low stresses. Linear elasticity is controlled by the cell edge bending or cell wall stretching if the material is closed cell. In the long collapse plateau, deformation of the cells occurs by elastic buckling in elastomeric foams (rubber for example), by plastically yielding in elastic-plastic materials (such as a metal) and by brittle crushing in brittle foams (ceramics, glasses). When the cells are completely collapsed, faces of the cells touch each other and applied stress compresses the compact solid itself and this results in rapid increase of the stress values as seen on the densification region of the curves.

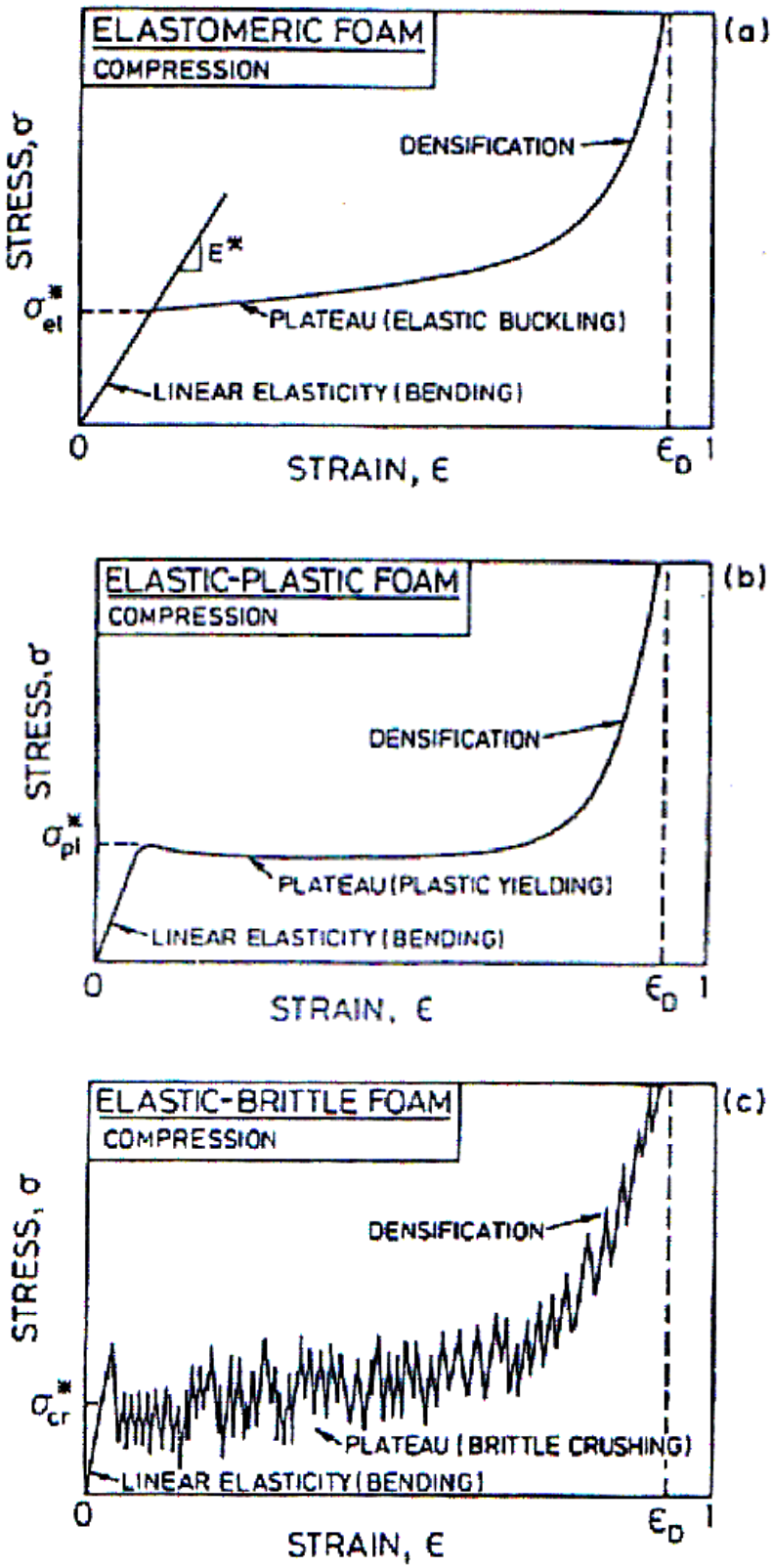

Figure 4.3. Compressive stress-strain curves of a) elastomeric, b) elastic-plastic and c) brittle foam [5].

Gibson and Ashby investigated the mechanical behavior of cellular materials. They developed a well-known theory to describe the relationship between the mechanical properties and the density of the cellular and cell wall materials by using a simple model and a number of experimental data [5]. Their theory is based on simple cubic model (Fig.4.4) and generalized equations are given below;

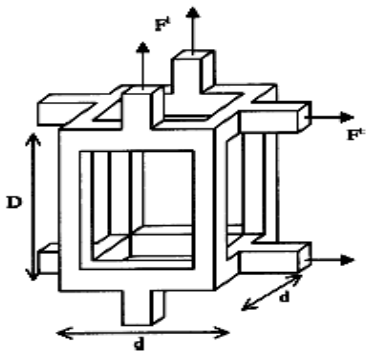

Figure 4.4. Simple cubic model [5].

$$\frac{E^*}{E_s} = C_1\left(\frac{\rho^*}{\rho_s}\right)^{\mu} \tag{4.1}$$

$$\frac{\sigma^*}{\sigma_s} = C_2\left(\frac{\rho^*}{\rho_s}\right)^{n} \tag{4.2}$$

Where σ^*, σ_s *are* the yield strength, ρ^* and ρ_s are the density, E^*, E_s are the young modulus of the porous material and solid cell wall, respectively. C_1 and C_2 are the proportionality constants and depend on the structure of the material. The exponents n and μ take different values for closed and open-cell materials, and for different deformation mechanisms. Gibson and Ashby have also compared the predictions of the Equations 4.1 and 4.2 with the experimental data obtained from a number of sources and found a good fit for regular isotropic materials [5]. For open-cell foams, n=1.5, whereas for closed-cell foams, n=1. However, the equations given above assume that deformation occurs primarily by beam bending. This is valid for open-cell foams, however, closed-cell foams may deform also by wall stretching, beam bending, or mixtures of the two [5, 29]. Experimentally, it was found that the elastic modulus changed with the relative density with the power of 1-4 for various structures based on equation 4.1. [30]. If the material is open cell or the cell walls are much thinner than the

cell edges the deformation takes place via edge-bending and *E* varies quadratically with the density, (μ=2) [31]. If the cell wall stretching is the dominant deformation behavior, μ=1. On the other hand, Gibson and Ashby showed that *E* can also vary cubicly as a function of density, μ=3, for closed cell materials [32].

The equations developed for the open cell materials take into account only the cell edge bending and predict the yield strength of open-cell and closed-cell materials where the cell edge bending is dominant. For closed cell foams the relation between relative density and the relative yield strength becomes more complicated due to the contribution of cell face stretching to the strength of material and also the fluid pressure in the closed cells. If we consider the fluid filled foam, the internal fluid pressure (p_0) is greater than atmospheric pressure (p_{atm}), the differences between p_0 and p_{atm} puts the cell walls in tension and there will be no buckling in the cell walls until it is overcome by the applied stress. So, for the closed cell materials relation between the elastic modulus and the relative density is described by Gibson and Ashby as given in the equation 4.3 [5].

$$\frac{E^*}{E_s} = \phi^2\left(\frac{\rho^*}{\rho_s}\right)^2 + (1-\phi)\frac{\rho^*}{\rho_s} \quad (closed\ cell) \tag{4.3}$$

Gibson and Ashby compared their predictions with a large number of experimental data and developed the open and closed cell equations for the elastomeric, elastic-plastic and brittle cellular materials. Deformation occurs in the elastomeric cellular material such as polyurethane and polyethylene foams in the form of elastic bending in the initial linear part and elastic buckling in the long plateau (Fig.4.3 a). Deformation is still recoverable in this region. Relation between the elastic collapse stress σ^*_{el}, modulus and the relative density can be predicted as below [5].

$$\frac{\sigma^*_{el}}{E_s} = 0.05\left(\frac{\rho^*}{\rho_s}\right)^2 \quad (open\ cell) \tag{4.4}$$

$$\frac{\sigma^*_{el}}{E_s} = 0.05\left(\frac{\rho^*}{\rho_s}\right)^2 + \frac{p_0 - p_{atm}}{E_s} \quad (closed\ cell) \tag{4.5}$$

The elastic-plastic materials such as rigid polymers and metals collapse plastically when loaded beyond the linear elastic regime. Plastic collapse occurs through the long deformation plateau (Fig.4.3 b) and material is permanently deformed. Variations of the strength with density for open and closed cell materials are given as;

$$\frac{\sigma_{pl}^{*}}{\sigma_{ys}} = 0.3\left(\frac{\rho^{*}}{\rho_{s}}\right)^{3/2} \quad (open\ cell) \tag{4.6}$$

$$\frac{\sigma_{pl}^{*}}{\sigma_{ys}} = 0.3\left(\phi\frac{\rho^{*}}{\rho_{s}}\right)^{3/2} + (1-\phi)\frac{\rho^{*}}{\rho_{s}} + \frac{p_{0} - p_{atm}}{\sigma_{ys}} \quad (closed\ cell) \tag{4.7}$$

Gibson and Ashby also analyzed crushing of brittle foams, such as ceramics, glasses and some brittle polymers and developed the relationship between the relative crushing stress (collapse stress) and relative density of the closed and open cell foams. According to their analysis the relationship between the relative crushing stress, σ^{*}_{cr} and density for open and closed cell materials are provided as below;

$$\frac{\sigma_{cr}^{*}}{\sigma_{ys}} = 0.2\left(\phi\frac{\rho^{*}}{\rho_{s}}\right)^{3/2} \quad (open\ cell) \tag{4.8}$$

$$\frac{\sigma_{cr}^{*}}{\sigma_{fs}} = 0.2\left(\phi\frac{\rho^{*}}{\rho_{s}}\right)^{3/2} + (1-\phi)\frac{\rho^{*}}{\rho_{s}} \quad (closed\ cell) \tag{4.9}$$

In these equations ϕ is in the range of;

$$\left(\frac{\rho_{m}}{\rho_{s}}\right) \leq \phi \leq 1$$

The term ϕ corresponds to the fraction of the solid present in the cell edges and the remaining fraction (1-ϕ) is in the cell walls in Gibson and Ashby model. The case of ϕ=1 corresponds to an open cell foam with material only in cell edges, lower values of ϕ corresponds to a foam with thicker cell walls and those for closed cell materials with negligible cell edges are given by ϕ=0. The first terms in all these equations developed for the closed-cell cellular materials describe the contribution of the cell beam bending to the strength and modulus, respectively, and are identical for both closed and open cell

foams. The second term includes the contribution of cell walls stretching, membrane effect, and does not exist for the case of open cell foams.

The complex dependence of the constants (C_1, C_2, n and μ for example described in the general equations 4.1 and 4.2) on microstructure is not known well. At the cellular scale being open or closed cell, the geometrical arrangement of the cell elements, e.g. angle of the intersections and the struts and the wall shapes of the cell such as curvature, cross sectional shape and uniformity have important effects on these constants. At large scale the geometrical arrangement of the cells is important, if they are periodic or disordered [33]. Most of the theoretical solutions have been done for simple three dimensional cell structures with straight struts or walls at low densities with periodic arrangement. However several recent studies about the cellular materials indicate that some refinements to earlier models are needed to account for discrepancies between predictions and experimental measurements of Young's modulus and compressive strength. But, for more complex random models, it is necessary to improve predictions for observation of the mechanical properties of real cellular solids. It was emphasized by Garboczi and Roberts that there are no exact analytical calculations available for random materials because it was very difficult to develop sufficiently accurate model of the microstructure, so that numerical methods become necessary [33].

Nieh *et al.* used images of aluminum foam and finite element method (FEM) to predict their modulus values [34]. FEM has been also used by Van der Burg *et.al.* to investigate the properties of three dimensional random open cell Voronoi tessellations [35]. Voronoi tessellation model describes the production of cellular materials by foaming. Randomly distributed seed points are the centers of the cells. Assuming a constant growth rate of a cell starting in the seed points, the cell walls will be located equidistant between two neighbour points (Fig.4.5). Since foaming is only one way of generating cellular materials it was needed to investigate different types of cellular structures to alternate the statistical models.

Garboczi and Roberts used FEM to estimate the elastic properties of different model random cellular solids with a range of densities [6]. They showed that the theoretical relationship between density and the elastic modulus is more complex especially for random cellular materials than the commonly referenced empirical relationship of the Gibson and Ashby. The cellular structure models given in Fig. 4.6 and 4.7 were digitized on grids of a sufficiently high resolution to capture the important details of the model. The finite element method (FEM) uses the variational formulation

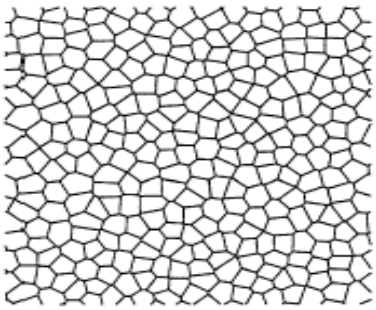

Figure 4.5. Voronoi tessellation [36].

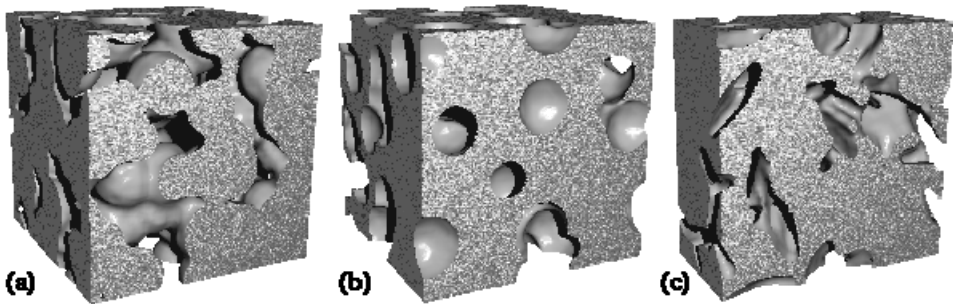

Figure 4.6. Boolean models of porous media. (a) overlapping solid sphere, (b) overlapping spherical pores and (c) overlapping ellipsoidal pores. [6]

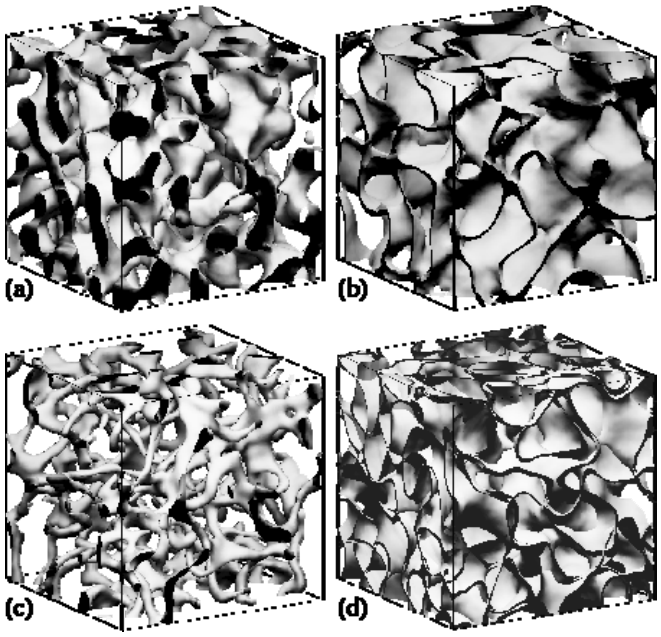

Figure 4.7. Three dimensional Gaussian random field models, (a) single cut, (b) two cut, (c) open-cell intersection and (d) closed-cell union [6].

of the linear elastic equations and finds the solution by minimizing the overall elastic energy of the system. The Young`s Modulus of the system was then determined from the overall stresses and strains.

They developed equation 4.10 given below which is used for describing the mechanical properties of materials with high densities and microstructures illustrated in Fig.4.6 and 4.7. They also determined the constants of the Gibson and Ashby`s simple model equation, $E^*/E_s=C(\rho^*/\rho_s)$ for low density material models. In Table.1 constants of the predicted equations were tabulated.

$$\frac{E^*}{E_s}=\left(\frac{p-p_0}{1-p_0}\right)^m, \quad \left(p=\frac{\rho^*}{\rho_s}\right) \tag{4.10}$$

Table 1. Parameters correspond to the described models. [6]

	$p<p_{max}$			$p>p_{min}$		
Fig.	n	C	p_{max}	m	p_0	p_{min}
4.6 (a)				2.23	0.348	0.50
4.6 (b)				1.65	0.182	0.50
4.6 (c)				2.35	0.202	0.50
4.7 (a)				1.64	0.214	0.30
4.7 (b)	1.58	0.717	0.50	2.09	-0.064	0.10
4.7 (c)	3.15	4.2	0.20	2.15	0.029	0.20
4.7 (d)	1.54	0.694	0.40	2.30	-0.121	0.15

The porous materials developed in this study are PMMA based materials that have randomly distributed cells with irregular cell shapes and sizes. The predictions of Roberts and Garboczi for the relation of modulus with density may be more realistic for these materials. The prepared structures have some similar microstructure developed in the model with the name of “overlapping solid spheres” shown in Fig. 4.6 (a). The relative density of the materials is also in the limitations of the models.

Chapter 5
EXPERIMENTAL

5.1. Materials

The PMMA based porous plastic mold materials were produced by the polymerization of water-in-oil emulsion from hardenable composition containing methyl methacrylate (MMA-$C_5H_8O_2$, Degussa, Germany), polymethyl methacrylate beads (PMMA, Keramische Laufen, Germany), dibenzoyl peroxide (BPO-$C_{14}H_{10}O_4$) as initiator of the polymerization reaction (Peroxid-Chemie GmbH), emulsifier (Keramische Laufen, Germany) and water. PMMA beads with various average bead sizes in the range of 22 and 157 μm were used as filler material. To provide the homogeneity and the stability of the emulsion, water-soluble nonionic surfactant of ethylene oxide-propylene oxide (EO-PO) block-copolymer was used.

5.2. Characterization of Materials

For the characterization of the emulsion constituents, Fourier Transfer Infrared Spectroscopy (FT-IR), Differential Scanning Calorimetry (DSC), and Scanning Electron Microscopy Techniques (SEM) were used.

5.2.1. Fourier Transform Infrared Spectroscopy

FT-IR spectrometer (Shimadzu) was used with the resolution of 2 cm^{-1} in the wavenumber range of 400-4600. For the FT-IR analysis of the powder materials, about 0.005 gr sample was mixed with powder KBr to prepare the pellets. For the analysis of liquid MMA, KBr pellets were prepared and MMA was dropped onto them.

FT-IR spectroscopy is one of the most powerful tools for identifying and investigating hydrogen bonding in polymers and is used for defining the polymer systems. Figs.5.1 (a) and (b) show the FT-IR spectrum of the filler PMMA beads with average particle diameters of 150 μm and 35 μm, respectively. These datas were used to identify the origin of the beads. In Fig 5.1 (c) FT-IR spectrum of MMA is also given. In these figures, some characteristic bonds of methyl methacrylic are seen. In the graphs,

bonds approximately at 1750, 1280 and 1150 cm^{-1} corresponding to C=O, C–O and C–O–C stretching of carboxylic group (O–C=O), respectively are observed. Bands nearly at 1400 and 1490 cm^{-1} corresponding to CH_3 and CH_2 bending and stretching and at 2983 cm^{-1} are result of the $–CH_3$ stretching. The frequencies at 990 and 750 cm^{-1} are assigned to CH_2 twisting and bending.

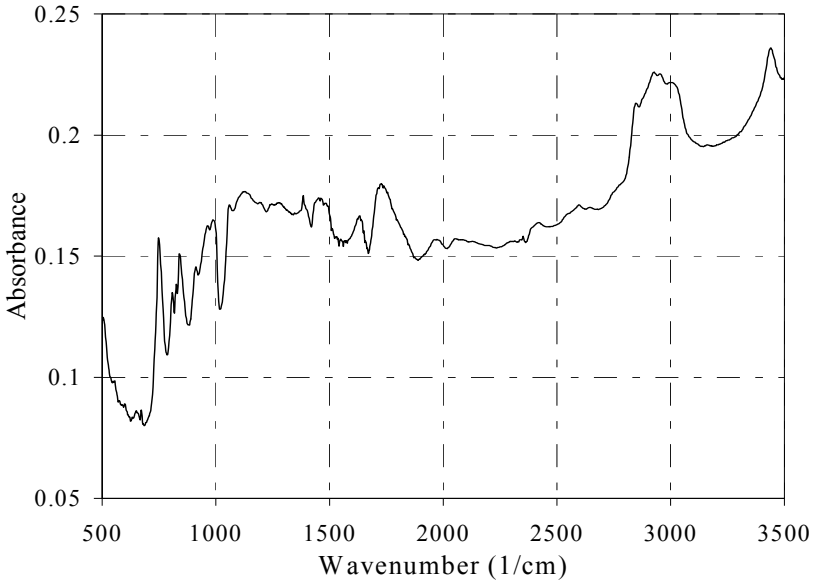

(a)

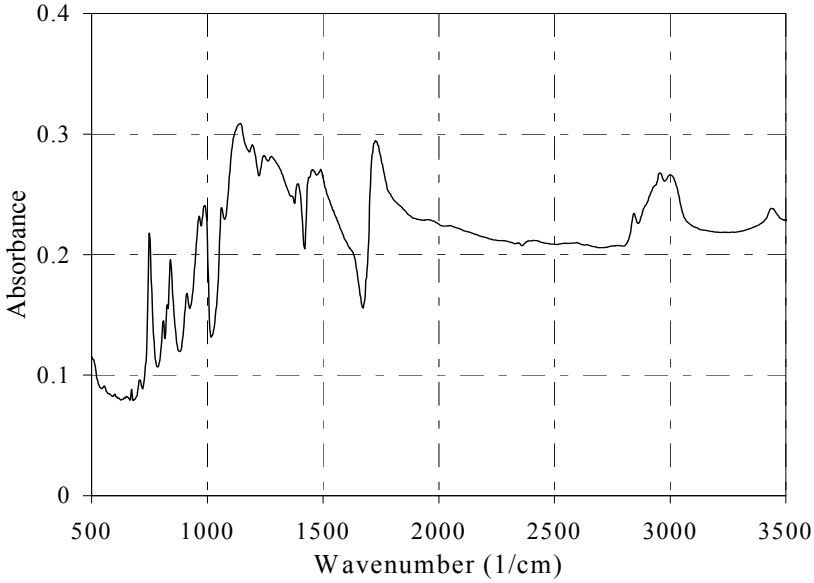

(b)

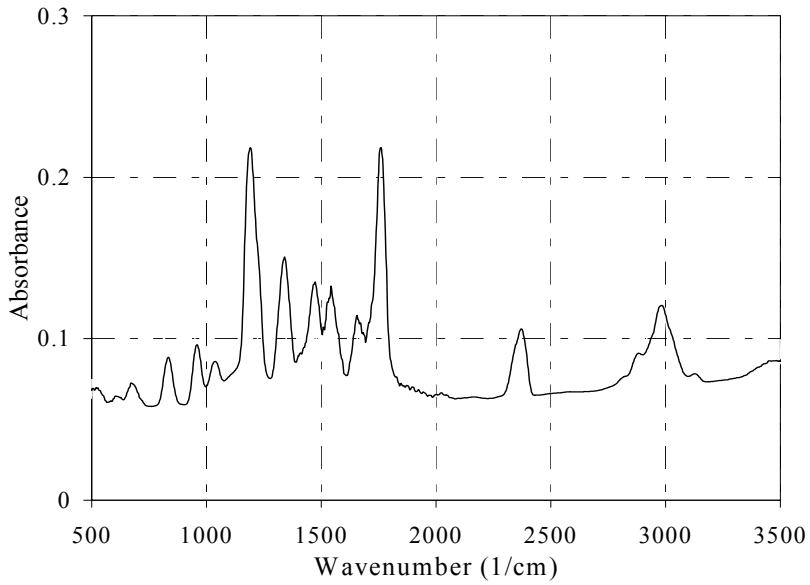

(c)

Figure 5.1. FT-IR spectra of PMMA beads with the average particle size of a) 150 μm b) 35 μm and c) methyl methacrylate monomer.

FT-IR spectrum of produced porous plastic materials is given in Fig.5.2, the characteristic bands of methyl methacrylate can be seen. The peak at nearly 2350 cm^{-1} is a result of the moisture content of the material.

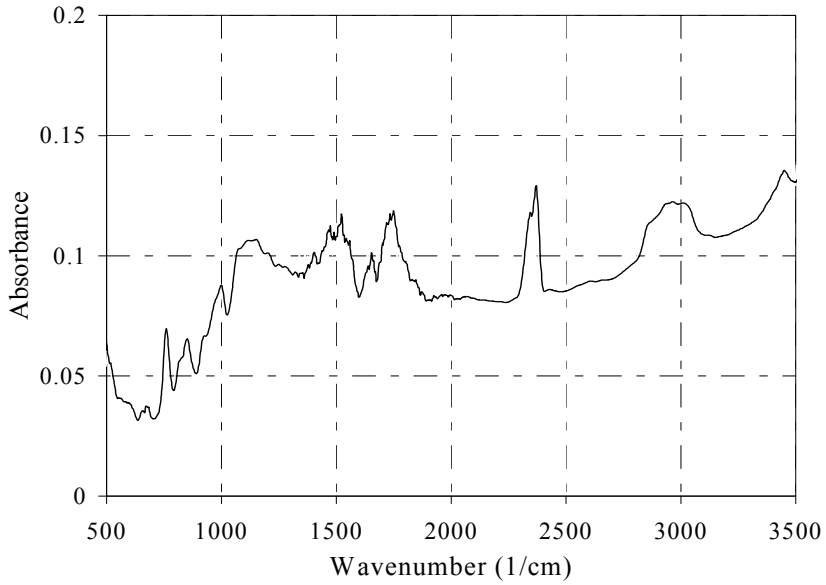

Figure 5.2. FT-IR Spectrum of produced PMMA–based porous plastic materials

5.2.2. Differential Scanning Calorimetry (DSC)

Calorimetric measurements were made with heating and cooling rate of 5 ^{0}C/min using a DSC (Shimadzu) under a nitrogen atmosphere. The temperature range analyzed was from 22 to 300 ^{0}C. Fig. 5.3 shows the DSC analysis results of PMMA filler beads. The exact temperature at which the polymer chains undergo change in mobility with the effects of given heat is called as glass transition temperature (T_g) and depends on the structure of the polymer. It is a unique property for amorphous polymers. PMMA is an amorphous polymer. It is hard and glassy under T_g. If the polymer is heated above its T_g, it becomes rubbery and this gives softness and flexibility to the polymer. As seen in the figures, beads exhibits glass transition temperatures (T_g) at about 113 ^{0}C.

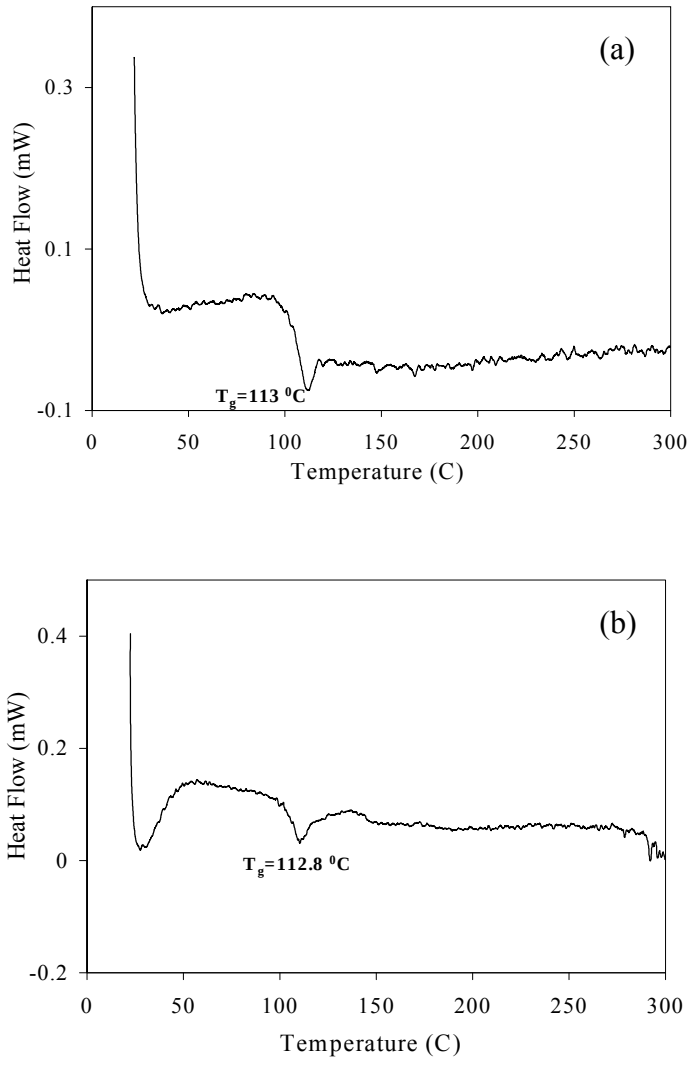

Figure 5.3. DSC profiles of PMMA beads with the average particle size of a) 150 μm and b) 35 μm.

Fig. 5.4 shows the DSC curve of BPO and it has a crystallization temperature (T_c) of 58.5 ^{0}C and an endothermic melting peak (T_m) at 118.6 ^{0}C.

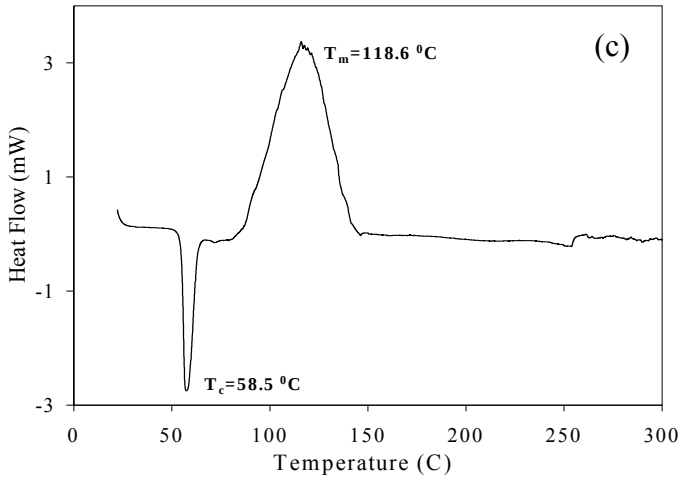

Figure 5.4. DSC profile of Dibenzoyl Peroxide (BPO)

5.2.3. PMMA Beads

Fig 5.5 and 5.6 show the SEM images of the filler PMMA beads with the average particle sizes of 157 µm and 35 µm, respectively. SEM images were used for the determination of the average particle sizes of the PMMA beads. It was also seen that there were some dissimilarities on the surfaces of the beads. The surfaces of the PMMA beads shown in Fig 5.6 have been plastized with dibutyl phatalate to assist the monomer absorption on the surface.

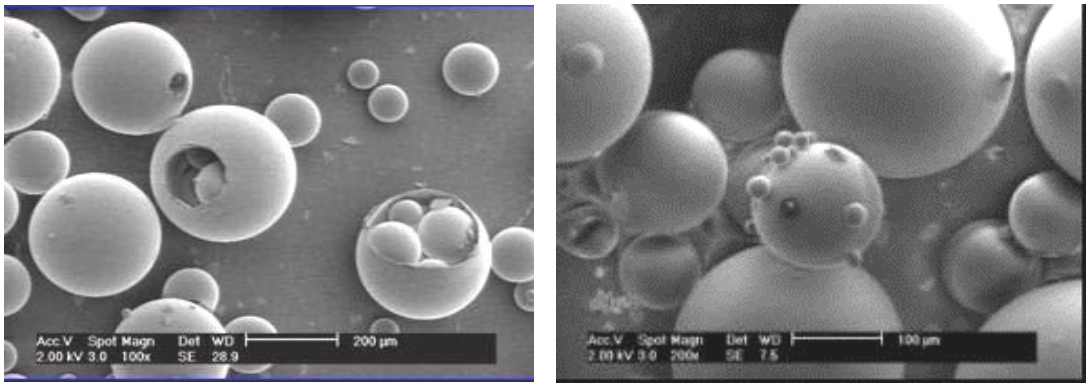

Figure 5.5. SEM micrographs of PMMA beads with average particle diameter of 157µm

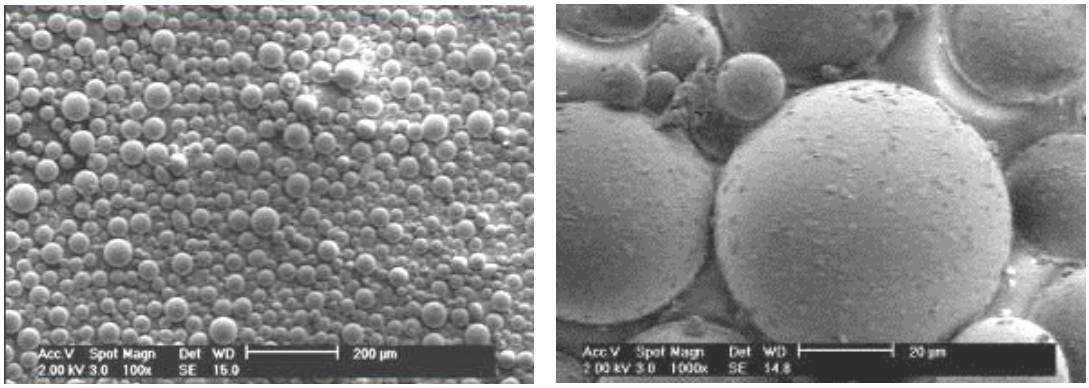

Figure 5.6. SEM micrographs of plastized PMMA beads with average particle diameter of 35µm.

5.3. Production of PMMA-Based Porous Plastic Mold Materials

In this study, PMMA-based plastic materials were produced by water-in-oil emulsion polymerization from a hardenable composition that contains water and monomer phases with the following concentrations. The water phase contained finer PMMA beads (20-30 wt.%) suspended in the blend of water and the surfactant. During the preparation of emulsions, water/surfactant ratio was kept constant (1/3) while their total concentrations varied between 30-40 wt.%. The monomer phase was contained the coarser beads (15-25 wt.%), dibenzoyl peroxide (0.3-0.5 wt.%) and methyl methacrylate monomer (15-20 wt.%). Monomer phase was stirred shortly and the blend formed a viscous solution of polymer in monomer due to the absorption of MMA by PMMA beads and the dissolution of beads surfaces. These two solutions were mixed together for very short period of time until the homogeneous emulsion was obtained and then cast on an epoxy mold with a smooth surface. Final emulsion consists of an immiscible water phase dispersed in monomer phase and additionally PMMA beads suspended in the emulsion.

After the polymerization is completed, the cast material is demolded and washed with tap water to remove remaining monomer and surfactant molecules. The described technique results in randomly distributed open cell macropore structure with an irregular morphology.

In addition, to evaluate the compressive properties and density values of the cell wall material, materials were produced without addition of water and the surfactant to the emulsion system and PMMA-based plastics, with nearly no porosity were obtained.

5.4. Incorporation of Nano Particles into the Emulsion

Addition of filler particles to the polymeric systems may result in improved properties such as higher mechanical properties of the produced materials. Due to the importance of mechanical durability of porous mold materials under high pressure, it was attempted to investigate the mechanical properties of the materials with the additional reinforcement particles. For this purpose, plastic materials were produced with additional clay (Na^+-montmorillonite (Na^+-MMT)), particles. The particles were purchased from Aldrich.

Fig.5.7 shows the idealized structure for montmorillonite; two tetrahedral sheets and between them an edge-shared octahedral sheet of either aluminum or magnesium hydroxide. Isomorphic substitutions in the tetrahedral lattice and the octahedral sheet cause an excess of negative charges within the montmorillonite layers, which are naturally balanced by exchangeable inorganic cations, such as Na^+ and Ca^{++}. The polar Si-O groups at the montmorillonite surface impart hydrophilic nature and these results in affinity of montmorillonite to polar molecules. Clay is needed to be organophilic in order to disperse in monomer phase (non-polar). Before using in emulsion systems clay should become organophilic by treatment with suitable modifiers.

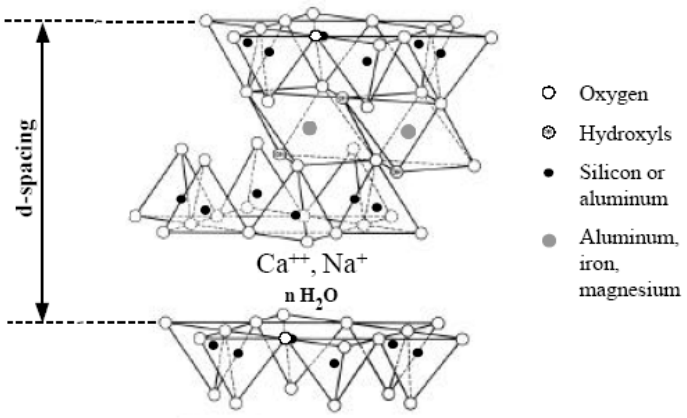

Figure 5.7. Crystal structure of montmorillonite. [37]

5.4.1. Modification of Clay

20 gr of Na^+-MMT was dispersed in 400 ml deionized water. A solution of hexadecyltrimethylammonium chloride (CTAC, $(CH_2)_{15}N(CH_3)_3^+$-Cl^-, Aldrich - 0,047 mol) and hydrochloric acid (HCl, 0,048 N) in 100 ml deionized water was prepared.

These two solutions were mixed and stirred for 1.5 hour at 75 ^{0}C (Fig.5.8). Organophilic MMT was formed by cationic exchange between Na^+-MMT galleries and hexadecyltrimethylammonium chloride in the suspension (Fig.5.9). With the penetration of alkylammonium ion into the galleries, distance within the galleries increases and by the affinity of the long hydrophobic polymer chain to non-polar molecules montmorillonite became organophilic at the end of the modification step. Then the suspension was filtered and the solid residue was washed with deionised water until no residual chloride was obtained by using the silver nitrate test. The product was dried in a fan oven at 70 ^{0}C for 24 hours and sieved before usage.

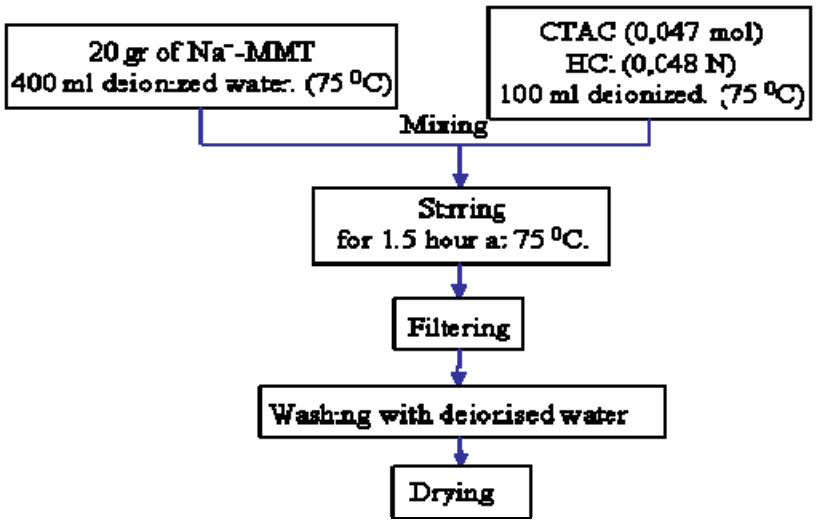

Figure 5.8. Modification steps of clay.

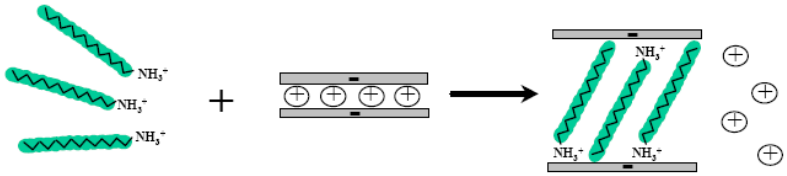

Figure 5.9. Cation exchange process between montmorillonite galleries and alkylammonium ions.

5.4.2. Production of Porous Plastic Material with Nano Particles

Almost the same procedure described in section was used for the production of reinforced plastic material. The main difference was that the MMA was mixed with clay and stirred for 2 hours before using it in the general procedure. To investigate the

modification effects of the clay particles, plastic materials were produced with modified (OMMT) and unmodified (MMT) montmorillonite.

5.5. Characterization of Mold Materials

Produced porous plastic materials were characterized to obtain their microstructural features, water permeability and mechanical properties.

5.5.1. Microstructure Characterization and Porosity Determination

To investigate the microstructural properties such as pore morphology and fractions, optical and scanning electron microscopy (SEM) techniques were used. Specimens were prepared for the microstructure investigations by cold molding, grinding and polishing. Optical micrographs of the specimens were taken at 50X magnification from at least seven different regions of the prepared surfaces for each specimen to obtain the best representative images of the structure to measure the porosity of the specimens. Thresholds of the optical micrographs were analyzed using Scion^{TM} image analyzer software. Fig.5.10 is an example showing the optical micrograph of a specimen and its threshold. The software measures the areas colored with black and by dividing this value with the total area the areal pore fraction was determined.

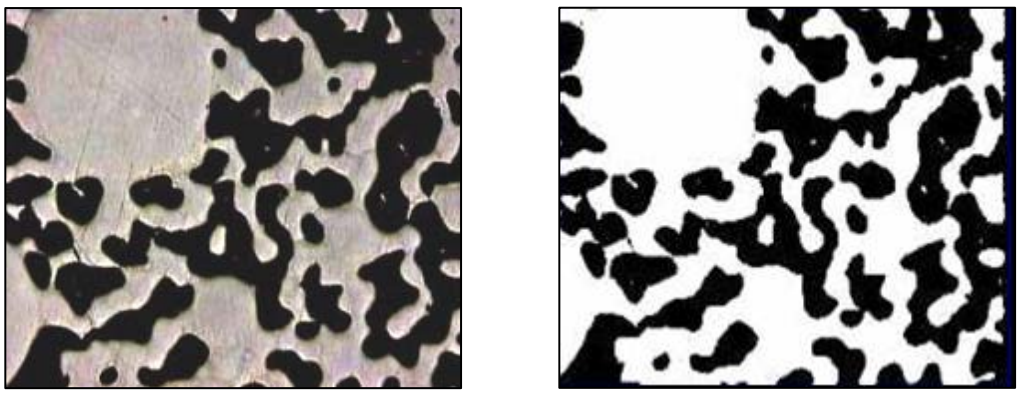

(a) (b)

Figure 5.10. a) Optical micrograph of the cross section of a specimen and b) the threshold of the same image in (a).

5.5.2. Water Permeability Test

The water permeability of the samples was measured using a custom made cylindrical permeability apparatus (Fig.5.11), with a diameter of 70 mm and depth of 20 mm. The apparatus is designed such that no water leakage occurs from the side surfaces. To get the permeation of water, 4 bar pressure was applied on the samples and volume of water permeated as a function of time was recorded. Permeability constant, κ was calculated by the equation of Henry Darcy, which describes the flow through porous media [38].

$$\frac{Q}{A} = \frac{\kappa}{\eta}\frac{\Delta Pe}{L} \tag{5.1}$$

In the equation, Q is the volume of liquid permeated per unit time, A is the cross sectional area of the sample, η is the viscosity of the fluid, ΔPe is the external driving pressure and L is the thickness of the sample. κ is the permeability coefficient and has a unit of length squared.

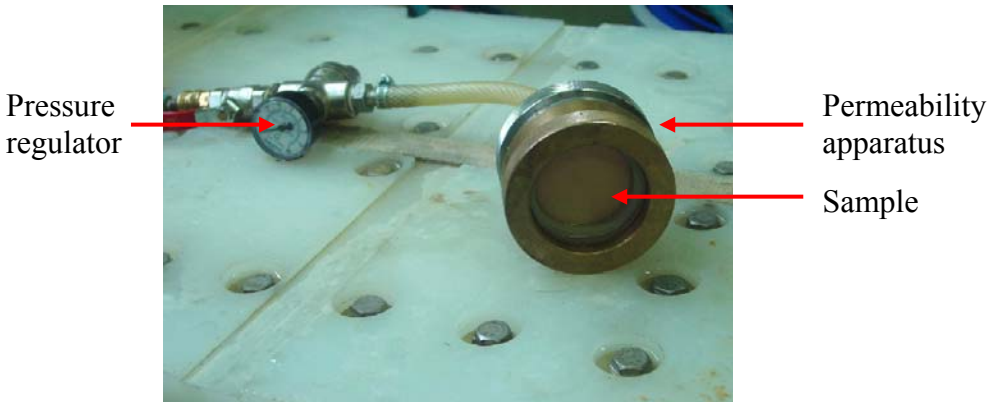

Figure 5.11. Water permeability apparatus.

5.5.3. Characterization of Mechanical Properties

5.5.3.1. Compression Test

Compressive mechanical tests were performed on the porous materials to investigate the effects of the pore morphology on the mechanical behavior, such as

collapse stress and elastic modulus. Specimens with 15 mm diameter and 20 mm length were sectioned from lager slabs and all the specimens were dried at 35^0C for 24 hours prior to testing. At least five specimens from each set were tested at room temperature and under a constant crosshead speed of 1.3 mm/min (strain rate of 0.001 s^{-1}), using a Shimadzu^{TM} universal testing machine (Fig.5.12). Compression test specimens were also used for density measurements. They were weighted after drying and by dividing weights to volume, densities of the materials were calculated.

Compressive stress values were calculated by dividing the load values to the surface area normal to the loading direction and strain values were obtained by dividing the stroke values with the initial length of the specimen. From the initial linear part of the compressive stress-strain graph elastic modulus values were calculated. Stress values at transition point from elastic to plastic deformation region give the collapse stress of the materials.

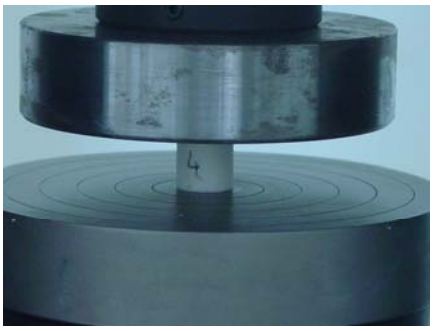

Figure 5.12. Compression test equipment

5.5.3.2. Fracture Toughness Measurement

Fracture toughness (K_{ic}) of PMMA based porous materials were measured according to ASTM D5045-91, based on single edge notch bend (SENB) specimen configuration [39]. Specimens with the thickness of 6 mm and width of 12 mm were prepared by sectioning from larger slabs using a diamond saw. On one edge of the specimens, a notch was opened by machining with a rotating abrasive disc and a sharp pre-crack was formed by simply pressing a sharp razor blade into the notched region [40]. All specimens were dried at 35^0C for 24 hours and toughness tests were performed at room temperature. Specimens were tested using the universal test machine with the crosshead speed of 10 mm/min. K_{ic} values were calculated based on the following equation in the units of MPa $m^{1/2}$.

$$K_{IC} = \left(P_Q B W^{1/2}\right) f(x) \qquad (5.2)$$

In the equation, P_Q, B, W and $f(x)$ are load, specimen thickness, specimen width and a calibration factor, respectively.

To investigate the fracture mechanism of the produced materials, fracture surface of the SENB specimens were analyzed by using SEM technique after fracture tests.

5.5.3.3. Determination of Residual Mechanical Properties after Cyclic Loading

Compressive cyclic loading tests were performed on the plastic materials to investigate the residual mechanical properties after repeated loading. Specimens with 15 mm diameter and 20 mm length were prepared and all the specimens were dried at 35^0C for 24 hours prior to testing. Specimens were repeatedly loaded for 1000 times under stress values of 9, 7.5 and 6 MPa (75%, 62.5% and 50% of the collapse stress values, respectively). Tests were performed at room temperature with the stress control conditions using the universal testing machine. After completion of the cyclic loading, the specimens were statically loaded to failure, under the same conditions of compression tests. After 1000 cycle loading, deformations in the structure and the variation in elastic modulus and collapse stress values were investigated.

Chapter 6
RESULTS AND DISCUSSION

6.1. Effects of Emulsion Constituent Concentrations on the Properties of Materials

6.1.1. Microstructure

PMMA-based porous plastics were produced with various concentrations of water-in-oil emulsion constituents. Fig.6.1 shows the SEM images of the porous materials processed with varying total weight fraction of water and surfactant in the emulsions (water/surfactant=1/3). The concentrations of these constituents in the emulsions were changed in the range of 29-40 wt.%. The results showed that the pore fraction, morphology and cell connectivity are significantly affected by the total concentrations of water and surfactant. It was observed that the amount of water in the emulsion is directly related to the pore fraction and connectivity. As the concentrations of these constituents are increased, the porosity and cell connectivity increases. The ratio between the concentrations of liquid constituent (-water/surfactant and monomer-) defines the formation of the network and also connectivity of the cells. At low concentrations of the water-surfactant, water droplets are completely enclosed by the oil phase and larger isolated pores are formed as illustrated in Fig.6.1 (a) Note that the free radical polymerization reaction occurs in the oil phase between MMA molecules that are activated by phenyl free radicals, which are a decomposition product of BPO. Polymerized monomer molecules form the cell walls with the contribution of PMMA beads. The macropore structure is mainly formed by the water droplets surrounded with surfactants within the emulsion during the polymerization of the oil phase. So, the homogeneous distribution of the water droplets and the stabilization of the emulsion through out the polymerization reaction are very critical for the microstructural properties of the material. As the polymerization is completed, the water phase is removed from the structure and open-cell porosity is left behind.

Fig. 6.2 (a) to (d) show the polished surface optical images of the plastic porous materials produced with various concentrations of monomer. The concentration of monomer in the emulsions was changed in the range of 12.5-20.8 wt%, respectively.

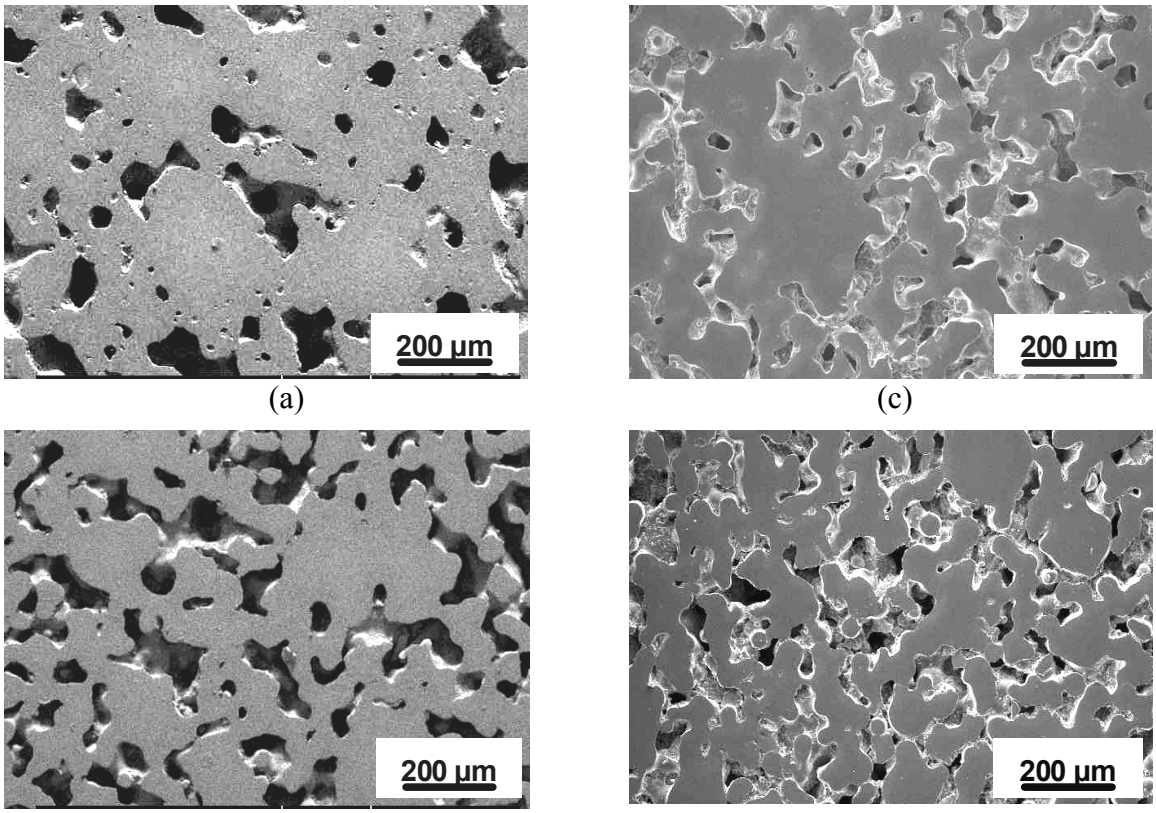

(a) (c)

(b) (d)

Figure 6.1. SEM micrographs polished surface of PMMA-based plastics, produced with various concentrations of surfactant/water. The total content of water and surfactant in the emulsions are 29, 33, 37 and 40 for a, b, c and d, respectively (water/surfactant=1/3).

As indicated in the figure, the pore morphology and cell structures are significantly affected by the concentrations of monomer. At high concentrations, larger isolated pores are formed. Additional amount of monomer accumulates around the filler beads and forms thicker cell walls with nearly no connectivity between the pores (Fig. 6.2 (d)). Lower concentration of monomer results in the formation of the material with microstructure that is given in Fig.6.2 (a) with higher connectivity. In this system, monomer molecules surrounding the PMMA beads form very thin connections between the beads.

In Fig.6.3 effects of emulsion liquid constituents on the microstructure of the porous plastic material is summarized by using a concentration diagram.

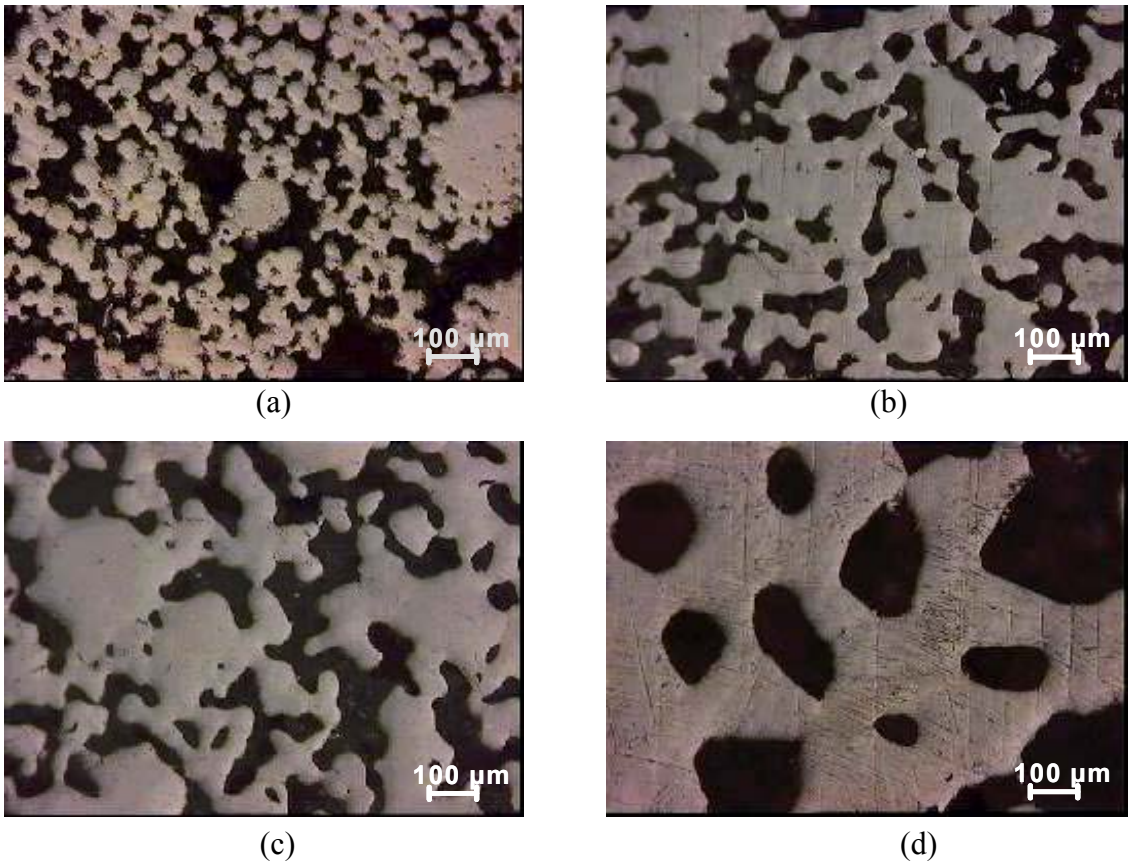

(a) (b)

(c) (d)

Figure 6.2. Optical polished surface micrographs of PMMA-based plastics, produced with various concentrations of monomer. The monomer content in the emulsions are 12.5, 18.3, 19.6 and 20.8 for a, b, c and d, respectively.

6.1.2. Porosity and Water Permeability

Fig.6.4 shows the variation of porosity and permeability constant as a function of total weight fraction of surfactant and water. As seen in this figure, the percentage of the porosity increases from 34 to 47% as the amount of water-surfactant increase from 29 to 40 wt.%, respectively. As the porosity and effective cell connectivity of the materials increases, the permeability constant of the specimens increases from 2.1 to 4.3 darcy for the given concentration range.

Increasing in monomer concentration up to a critical point has reverse effect on porosity and permeability as given in Fig. 6.5. It was found that as the monomer concentration increases from 12.5 to 19.6 wt%, the porosity is decreased from 46 to 34.5 %. However, the permeability constant is increasing from 2.7 to 3.4 darcy for the same concentration range. This is due to increased ratio of effective pores which are not in closed form and take a role in transportation of water.

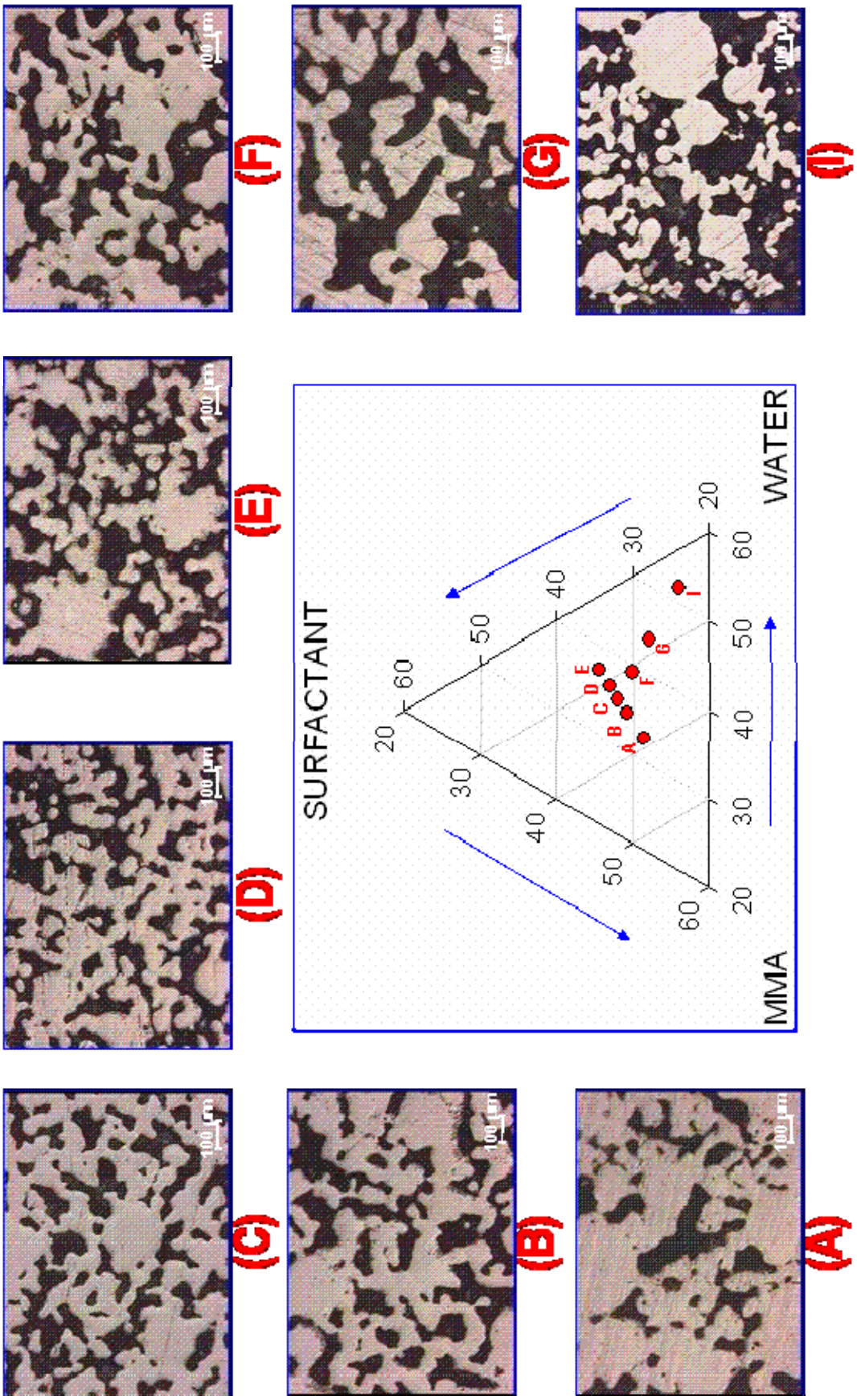

Figure 6.3. Effect of emulsion constituent concentrations on the microstructure

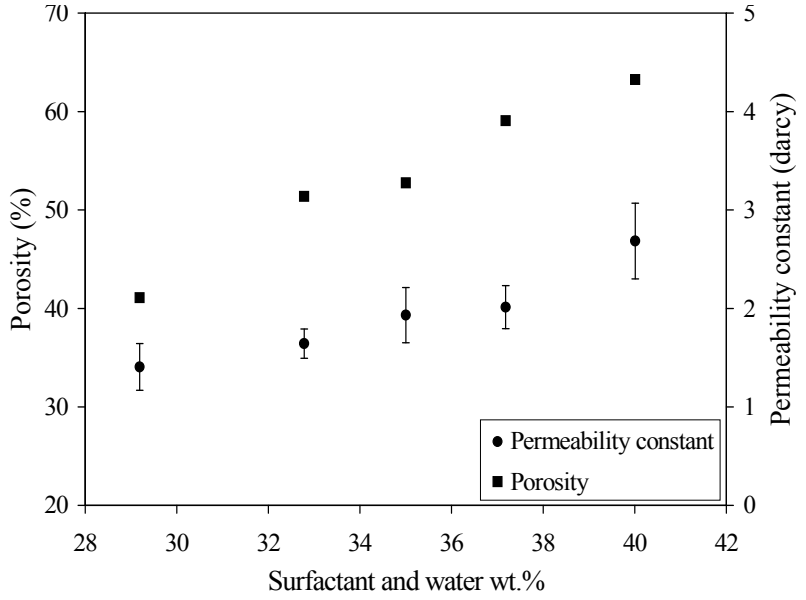

Figure 6.4. Porosity and water permeability constant of the PMMA-based porous plastics with respect to surfactant and water concentration (w/s=1/3).

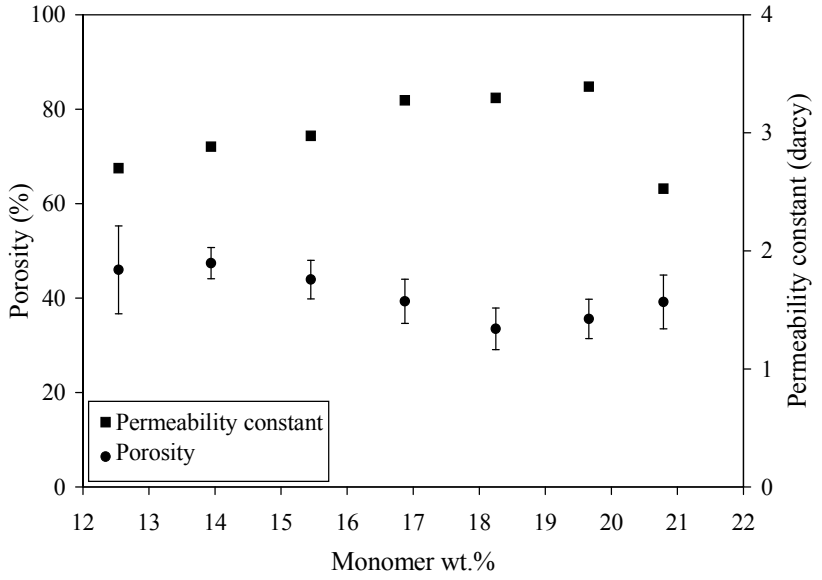

Figure 6.5. Porosity and water permeability constant of the PMMA-based porous plastics with respect to monomer concentration.

6.1.3. Mechanical Properties

Fig. 6.6 shows the compressive stress-strain graphs of the samples produced with various concentrations of water and surfactants (29 to 40 wt.%). The stress-strain

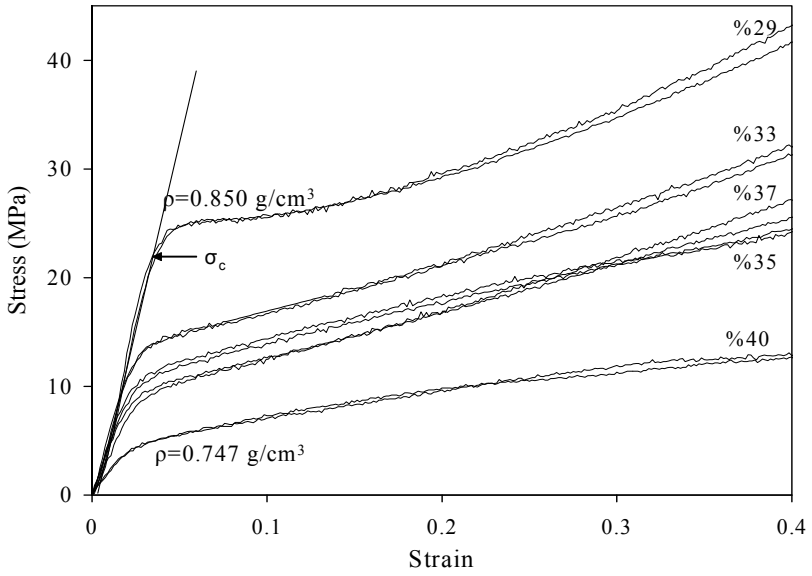

Figure 6.6. Compression stress-strain curve of materials with various surfactant and water concentrations (w/s=1/3).

behavior of all the specimens showed linear elasticity up to the collapse stress. The collapse stress (σ_c) is defined as the point at which deviation is observed in the linear part of the stress-strain curves. From the slope of the linear elastic region modulus values were also calculated.

Fig. 6.7 shows the variations in collapse stress and elastic modulus values with respect to water and surfactant concentrations. As seen in the figure, water and surfactant content has significant effect on the mechanical properties. It was found that the collapse stress and elastic modulus values decrease from 24 to 4.9 MPa and from 824 to 224 MPa, respectively, as the concentration of water-surfactant increases from 29 to 40 wt.%. Furthermore, densities of the tested materials change from 0.85 to 0.747 g/cm^3 for the given concentration range. As discussed previously, the material with a high density exhibited short deformation plateau (in region II) in the stress-strain graphs. This is associated with lower porosity and higher fraction of closed cells. On the other hand, as shown in Fig.6.6 material with a lower density has longer deformation plateau and material is completely collapse at high strain values. This is due to higher fraction of pores with open-cell structure that involves extensive progressive collapse of the pore network.

In addition to water-surfactant, effect of the MMA on the mechanical properties was investigated. Fig.6.8 shows the compression stress strain curves of the materials

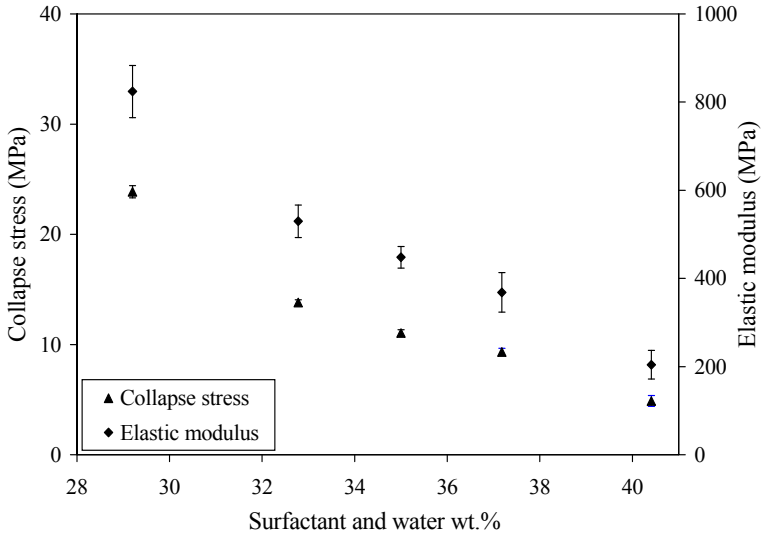

Figure 6.7. Collapse stress and elastic modulus of plastic mold samples with various surfactant and water concentration (w/s=1/3).

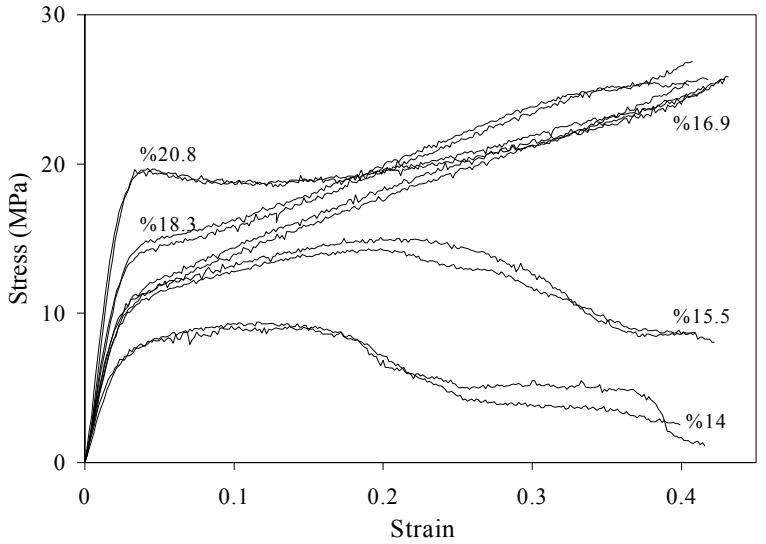

Figure 6.8. Compression stress-strain curve of materials with various monomer concentrations.

that were produced with various MMA concentrations. It can be observed from the figure that when the monomer concentration is under 16 %, the material has very short plastic deformation plateau and there is no densification, deformation is ended with the complete collapse of the material.

Fig.6.9 shows the variation of collapse stress and elastic modulus with respect to monomer concentration. The increase of monomer concentration in the range of 14-21% resulted in an increase of the collapse stress and modulus values from 8.4 to 19.3 MPa and from 356 to 687 MPa, respectively.

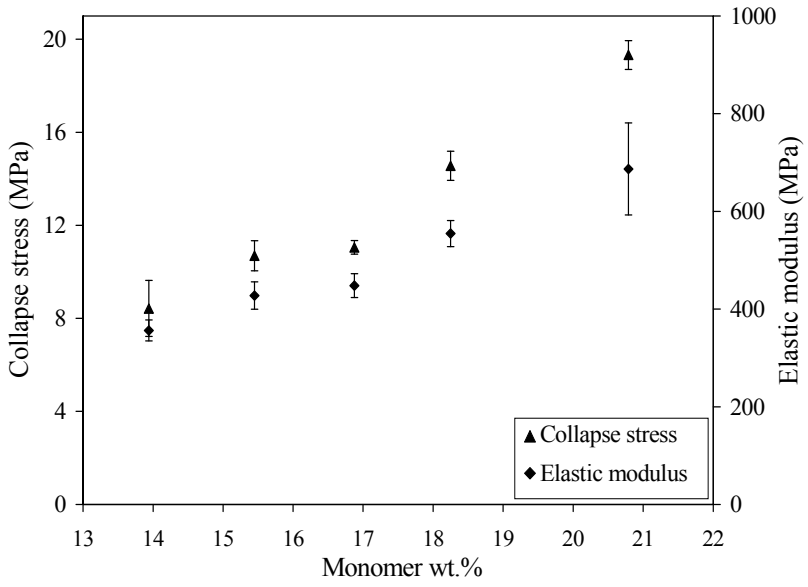

Figure 6.9. Collapse stress and elastic modulus of plastic mold samples with various monomer concentrations.

6.2. Effects of Average Particle Size of Fillers on the Properties of Plastic Porous Materials

6.2.1. Microstructure

In order to investigate the effects of particle size of the PMMA beads on the microstructure and performance of the porous plastic materials, samples were produced with various average particle diameters in the range of 22 and 157 μm. Figs. 6.10 (a), (b), (c) show the optical micrographs of the materials produced with the average particle diameter of 157, 88 and 22 μm, respectively. Incorporation of coarser beads results in formation of larger pores with higher fraction of porosity. Conversely, when finer particles are added into the emulsion, smaller pores occurs (Fig. 6.10(c)).

6.2.2. Porosity and Water Permeability

Fig. 6.11 shows the porosities and water permeability constants of the porous samples with various bead diameters. As the PMMA bead diameter increases from 22 to 130 μm, the percentage of porosity and hence the permeability values increase from 32 to 45% and from 2.2 to 4.2 darcy, respectively.

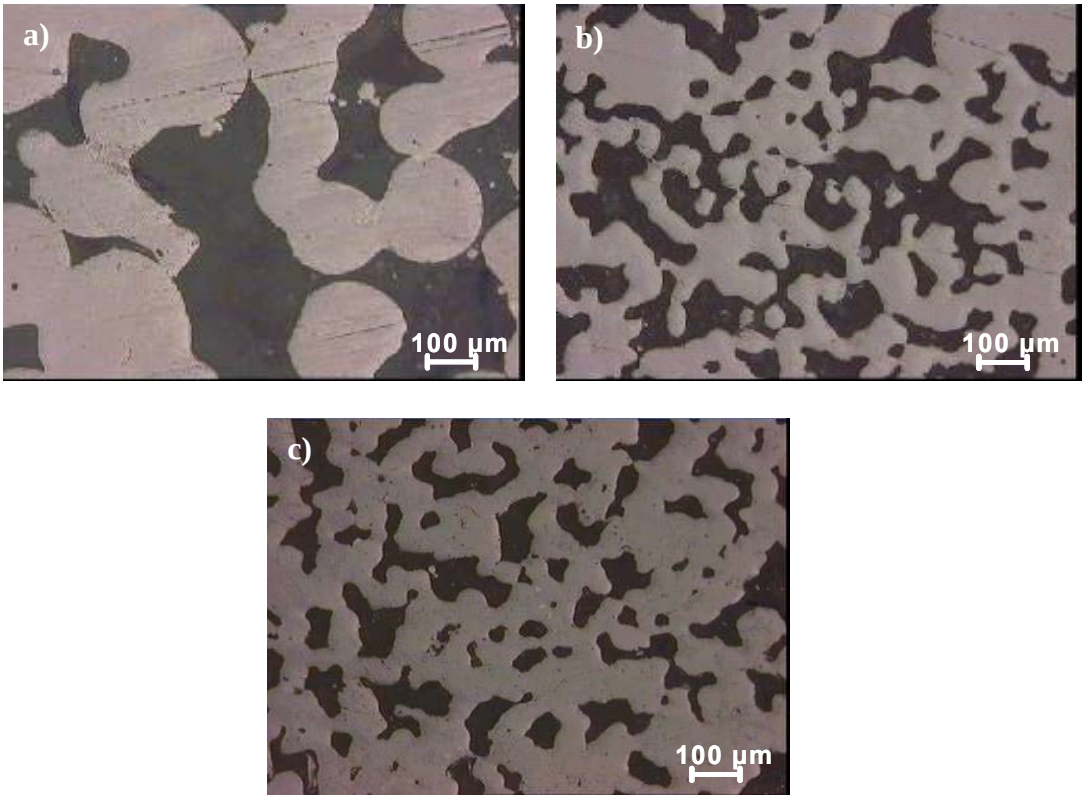

Figure 6.10. Optical images of PMMA-based plastics, produced with various average particle diameter of PMMA beads. The average particle diameters were 157, 88 and 22 μm for a, b and c, respectively.

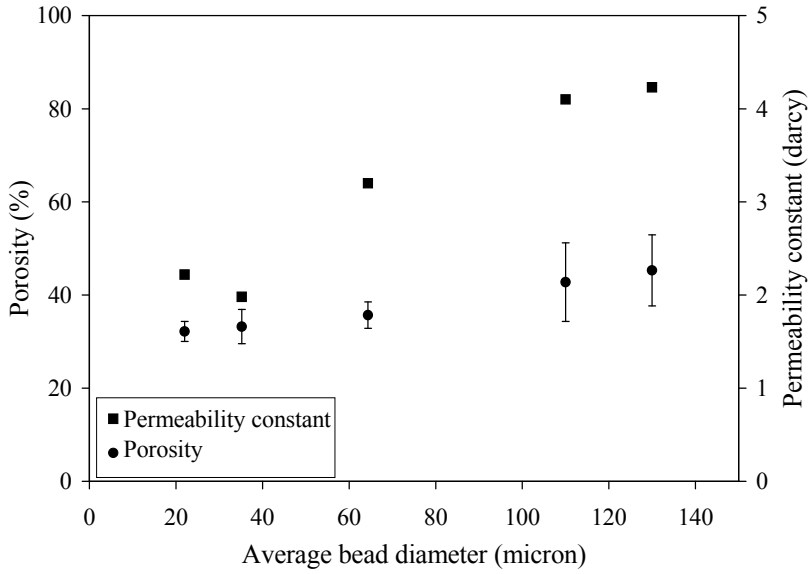

Figure 6.11. Porosity and water permeability constants of the PMMA-based porous plastics with respect to average diameter of the PMMA beads.

6.2.3. Mechanical Properties

Fig.6.12 shows the compressive stress-strain test results of the materials that were produced by using PMMA beads with various average bead diameters in the range of 22-130 μm. Fig. 6.13 shows the variation in collapse stress and elastic modulus values of the plastic porous materials with respect to average bead size of PMMA. For the variation of the diameters in this range, collapse stress and modulus values decrease from 17 to 7.3 MPa and 649 to 350 MPa, respectively. As it was mentioned above, coarser beads results in formation of larger pores and when the sufficient force for the collapse of the cell walls is applied, the material is deformed. Also, the bonding between the adjacent beads become weaker for the materials produced with coarser beads and this is also associated with the lower collapse stress values.

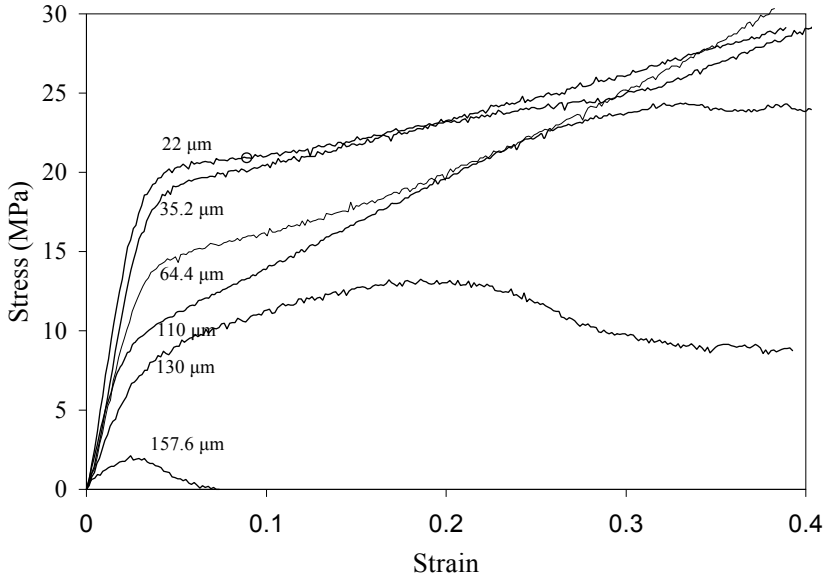

Figure 6.12. Compression stress-strain curve of materials with various average particle diameters of PMMA beads.

6.3. Effects of Nano Particles on the Properties of Materials

Fig.6.14 shows the X-Ray Diffraction analysis results of MMT and OMMT. As it can be observed from the figure, the structure of the montmorillonite is significantly affected from the modification process. Distance between the (001) basal planes increased from 14.8 Å to 19 Å.

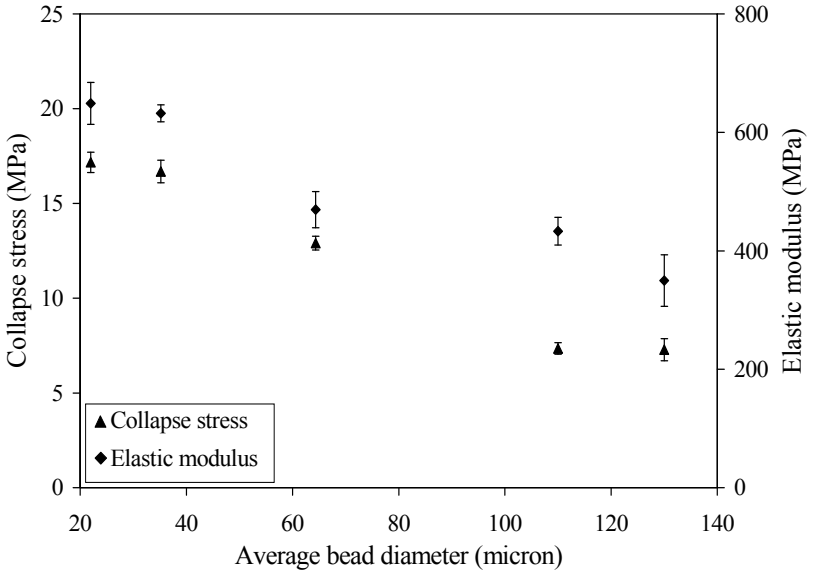

Figure 6.13. Collapse stress and elastic modulus of the PMMA-based porous plastics with respect to average diameter of the PMMA beads.

The results of the performed compression test results on the materials produced with OMMT and MMT are given in Fig.6.15. Results show that the produced materials with additional MMT particles have lower elastic modulus and collapse stress values. Using unmodified clay particles may be resulted in dissolution of particles in water phase and agglomeration of the particles because of weak wetting by monomer phase. Produced materials with the 1% of modified clay addition have improved mechanical properties, i.e.; about 90% increase in collapse stress and 50% increase in elastic modulus values. However, in the case of modified clay addition 2%, it was observed that there is no improvement on the mechanical properties. It is also known that amount of reinforcement addition is critical for the composite systems. In some cases, addition of reinforcement above the certain limits may decrease the strength of the materials.

Porosity and water permeability of the produced materials with additional clay particles were also measured and it was seen that addition of reinforcement particles has no significant effect on these properties.

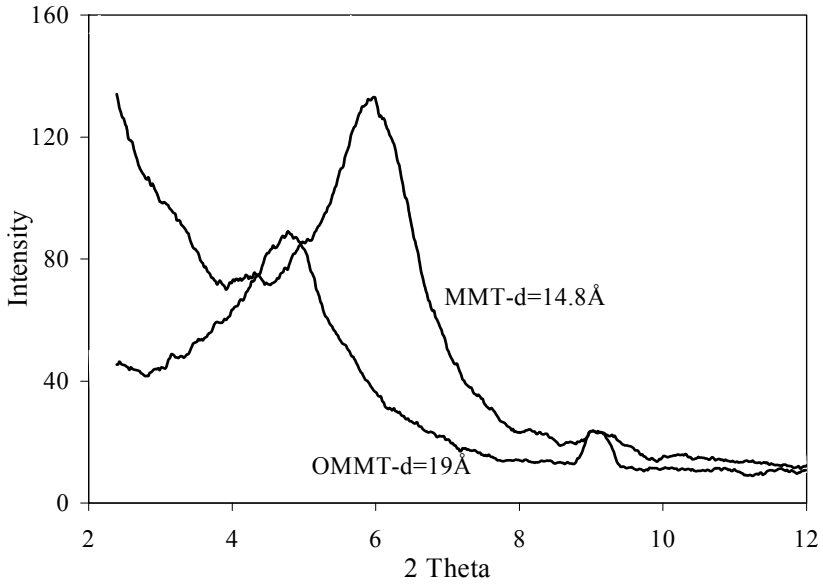

Figure 6.14. X-Ray Diffraction analysis results of MMT and OMMT.

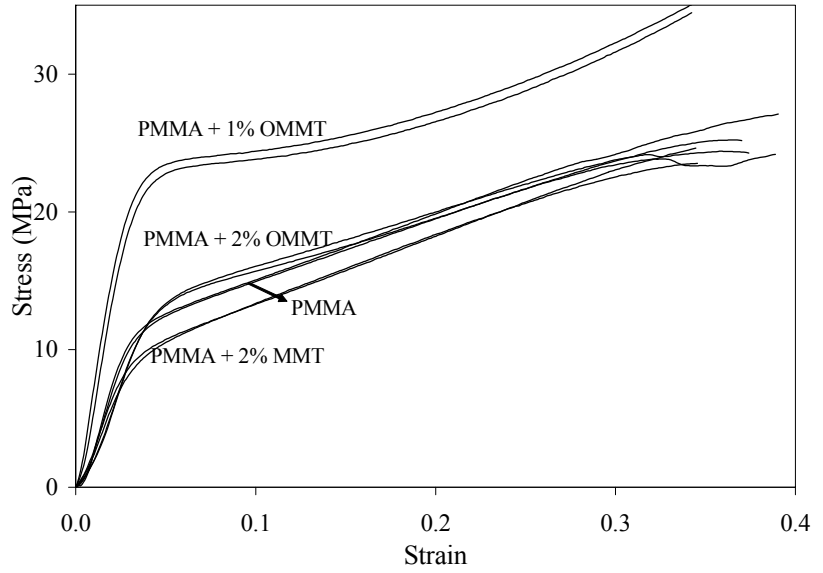

Figure 6.15. Compression stress-strain behaviors of specimens produced with additional MMT and OMMT particles.

6.4. Deformation Mechanism of PMMA-Based Porous Plastic Materials

6.4.1. Collapse Stress and Elastic Modulus

The mechanical performance of the produced material is critical since high pressure cyclic loadings are applied on these materials during the shaping of ceramic

articles. Mechanical behavior of porous materials during mechanical loading is significantly affected by the pore structure. The typical compressive stress-strain curve of a PMMA-based porous plastic processed in this study is shown in Fig.6.16. The graph exhibits three distinct regions, similar to the compressive behavior of elastic brittle foams described by Gibson and Ashby [5]. The first region is a linear elastic region that is controlled by cell wall bending and cell face stretching. The second region is a long deformation plateau with lower rate increasing stress values as compared to first region. Deformation in this region involves tearing and brittle crushing of the cells, progressive collapse of the pore network and plastic flow of the structure. This deformation plateau is generally described with an almost constant stress for open cell structure materials. With the collapse of the cells, opposing cell walls touch each other and further stress begins to compress the solid itself, and creates the final region of densification with a rapidly increasing stress (region III).

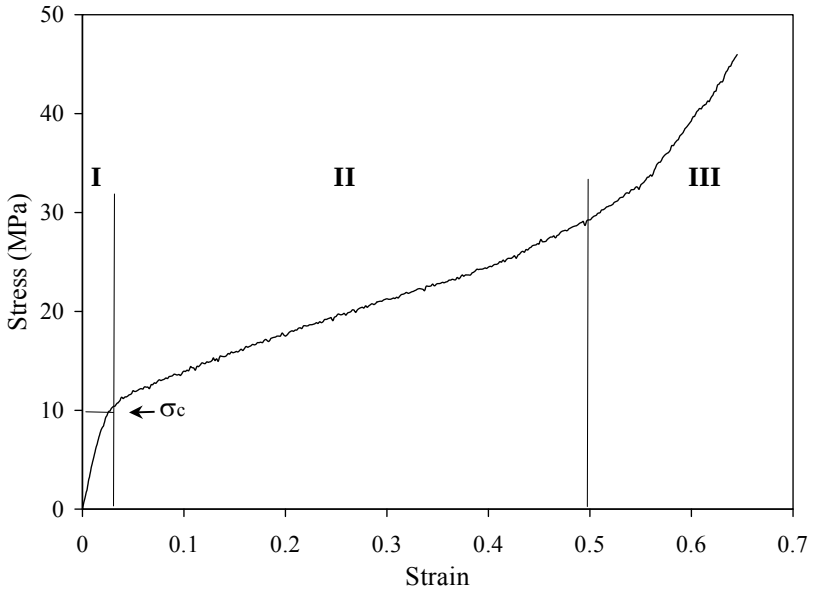

Figure 6.16. Typical compressive stress-strain response of PMMA-based porous materials

Gibson and Ashby described the second plateau region with nearly constant stress values for open-cell elastic brittle foams. The increase of stress level in the second region for the present case may be associated with the presence of a fraction of closed cells in the structure. Closed-cells cause to increase the contribution of the cell wall stiffness to the elastic modulus and increase in stress values in plastic deformation

plateau. The precise formation of the three region behavior depends on the cell structure and the density of the material. The material with a high density exhibited short deformation plateau (in region II) in the stress-strain graphs. As an example, Fig.6.6 shows the compression behavior of porous plastics with various porosity and densities. The material with a lower density has longer deformation plateau, such that densification begins at much higher strain values and for specimens with lowest density there is insignificant densification. This is due to higher fraction of pores with open-cell structure that involves extensive progressive collapse of the pore network for lower densities.

The collapse stress vs. density of the produced materials was predicted based on the analysis of Gibson and Ashby to compare with the experimental values. The produced materials fracture in brittle manner so the equation 4.9 for brittle materials were used. The distribution parameter given in Equation 4.3 and 4.9 can be estimated from the comparison of the experimental data and the predicted values of collapse stress (brittle-crushing strength) and elastic modulus [41-42]. For the comparison of the measured and predicted crushing strength of the specimens were normalized to the cell wall strength (σ_s= 1493.3 MPa) and foam density was normalized to cell wall density (ρ_s=1,124 g/cm^3). Note that the cell wall strength and densities were measured based on the non porous specimens that were made of without addition of water and surfactant. Fig. 6.17 shows the relation between relative crushing strength and relative density for the PMMA based porous materials. Straight lines on the plot are the predictions of the equation using trial values of ϕ. Comparisons indicate that the experimental data do not fit with the prediction of the developed equations of Gibson and Ashby.

Fig. 6.18 shows the variation of relative modulus as a function of relative density and the straight lines in the plot represent the predictions of the Equation 4.3. The equation for describing the relation between the relative density and the modulus is not valid for high density materials. It was obtained that the equations developed from the simple cubic model are not valid for the irregular cellular, high density materials.

The studied material has randomly distributed cells with irregular cell shapes similar to the described models given in Fig 4.6. The predictions given by Roberts and Garboczi which describes the properties of materials with high densities may be more realistic for the present materials. The constants within the equation were taken for the models given in Fig.4.6. Fig. 6.19 shows the comparison of the experimental data with

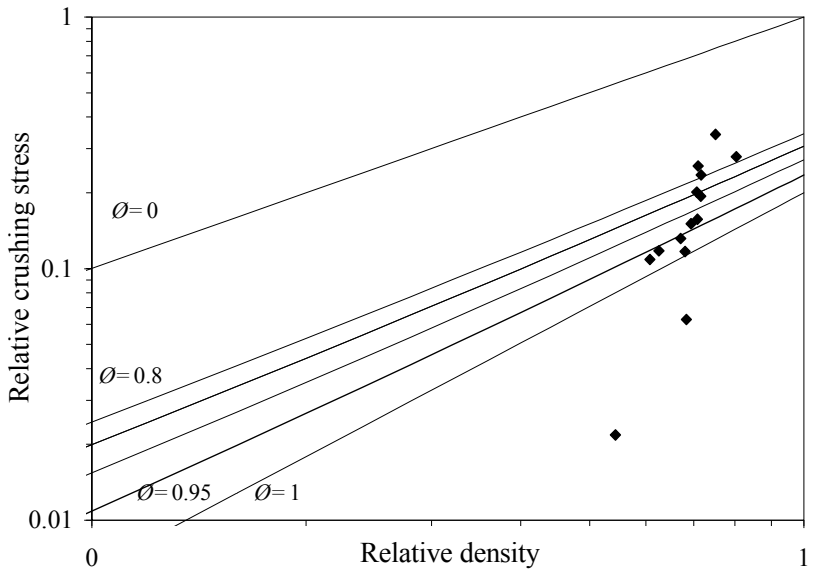

Figure 6.17. Variation of relative crushing stress as a function of relative density.

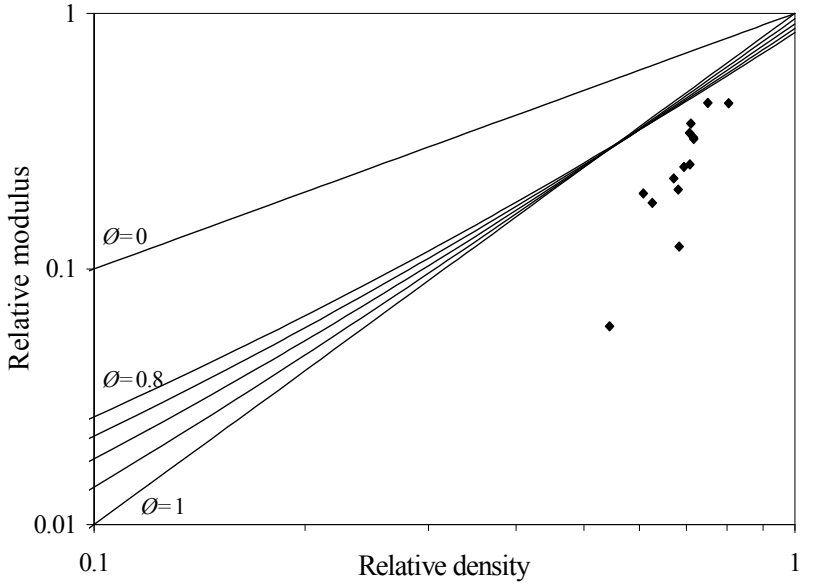

Figure 6.18. Variation of relative modulus as a function of relative density.

the predicted results of the Equation 4.10 for these models. As seen in the figure, the experimental data fits with the curve of the model called as "overlapping solid spheres" with the constants $p_0 = 0.348$ and $m = 2.23$ for the case of $p > p_{min}$ and $p_{min} = 0.5$.

6.4.2. Deformation Mechanism

To investigate deformation mechanism of the porous materials, compression tests were applied on the specimens at various stress levels below and over the collapse strength. As seen in the figure, the specimens loaded above the collapse stress of the

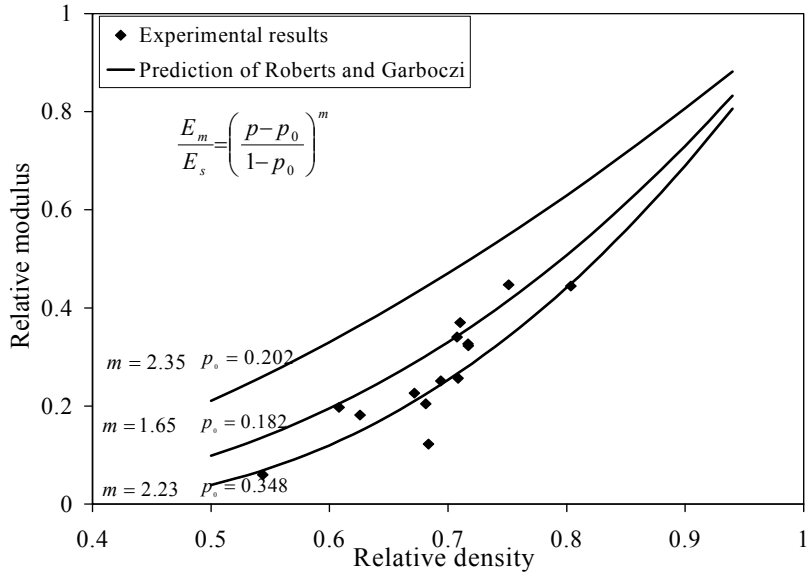

Figure 6.19. Comparison of experimental data and predictions of Garboczi and Roberts.

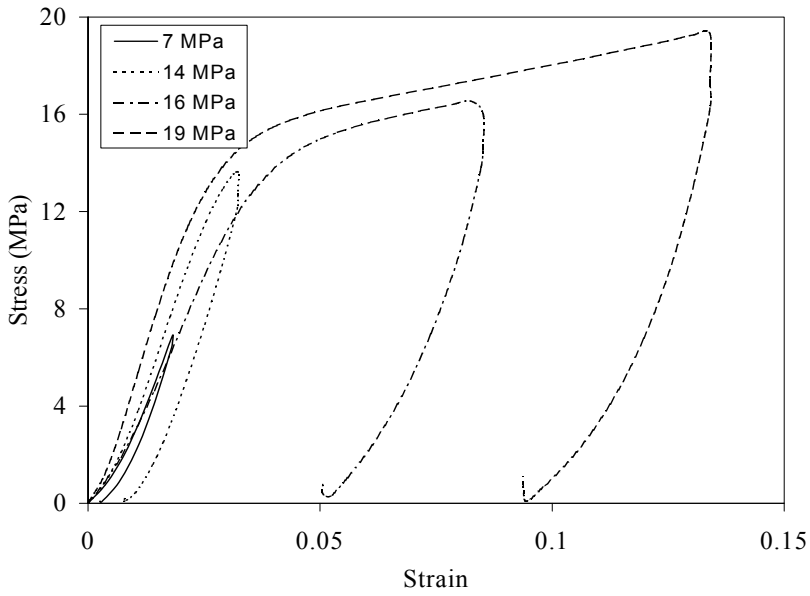

Figure 6.20. Stress strain curves of porous plastics loaded at the stress levels of 7, 14, 16 and 19 MPa.

material (≈ 12 MPa) some residual deformations occur. The residual deformation is associated with the failure of the cell structure.

Fig. 6.21 shows the cross section of the specimens unloaded and loaded to 7 MPa without delay. It was observed that there is no apparent deformation in the structure and material is elastically deformed for the stress values under the collapse strength.

However, for the specimens loaded at slightly over the collapse stress (loaded at 14 MPa), some residual deformations are visible. Cracking and cell bending are observed especially at thinner region of the cell walls as shown in Fig. 6.22.

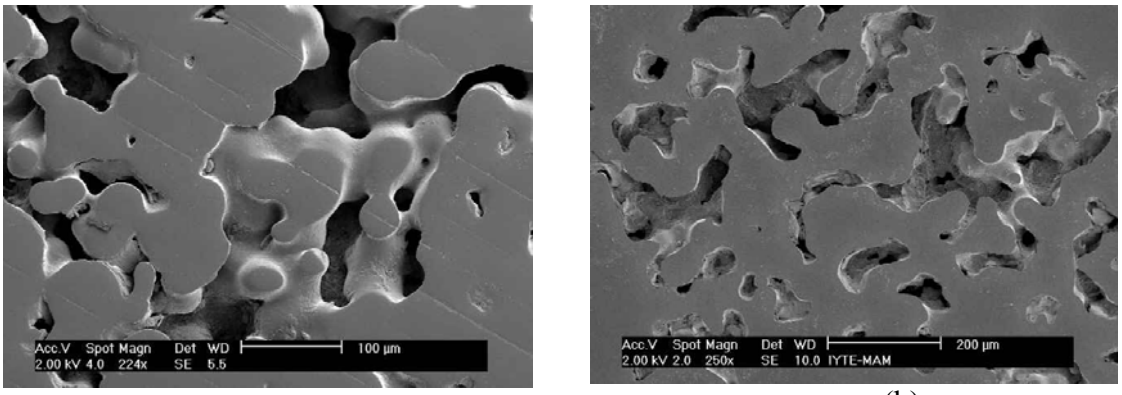

(a) (b)

Figure 6.21. SEM micrograph showing the cross section of the PMMA based porous plastic a) unloaded and b) after loaded at 7 MPa.

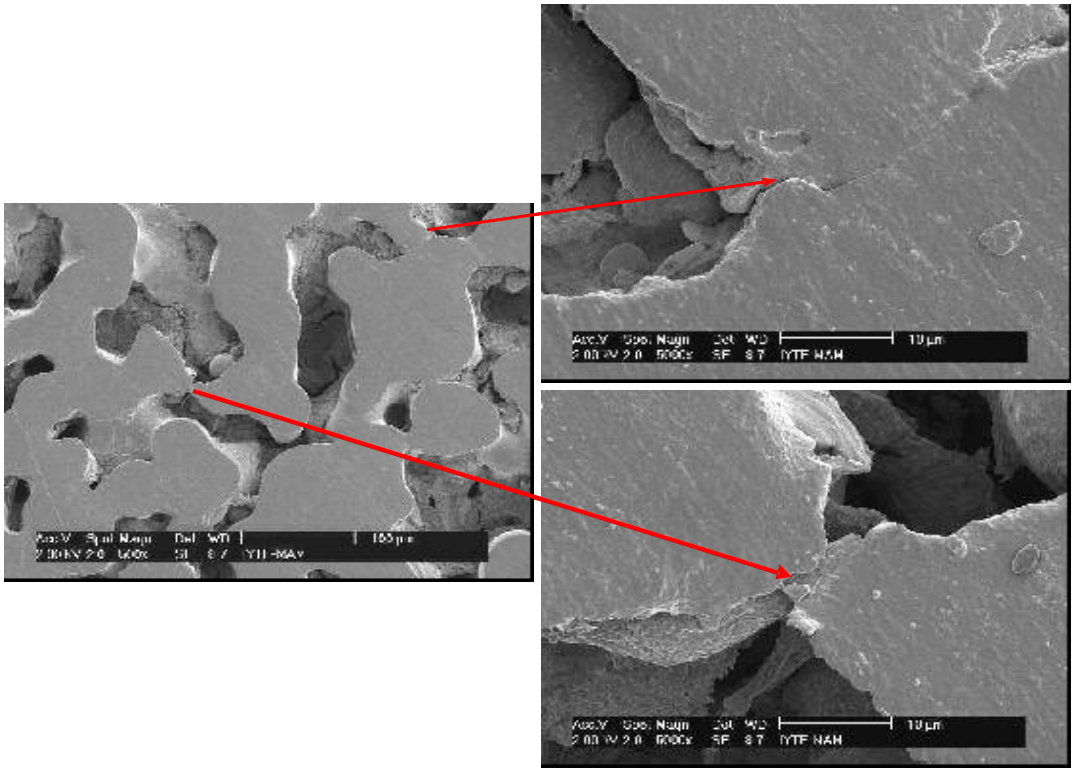

Figure 6.22. SEM micrograph of the porous plastics that were exposed to load-unload cycle at the stress level of 14 MPa.

Fig.6.23 shows the cross section of the specimens after loading at 19 MPa stress. This stress value is in the level of plastic deformation plateau of the material. Under the compression stress values relatively higher than the collapse stress, cell walls crack and failure in the brittle form occurs. Brittle fracture propagates through the weak points of the cells and densification occurs due to collapse of the cells and joining of cell walls. In Fig. 6.23 at higher magnifications completely collapsed cells are seen.

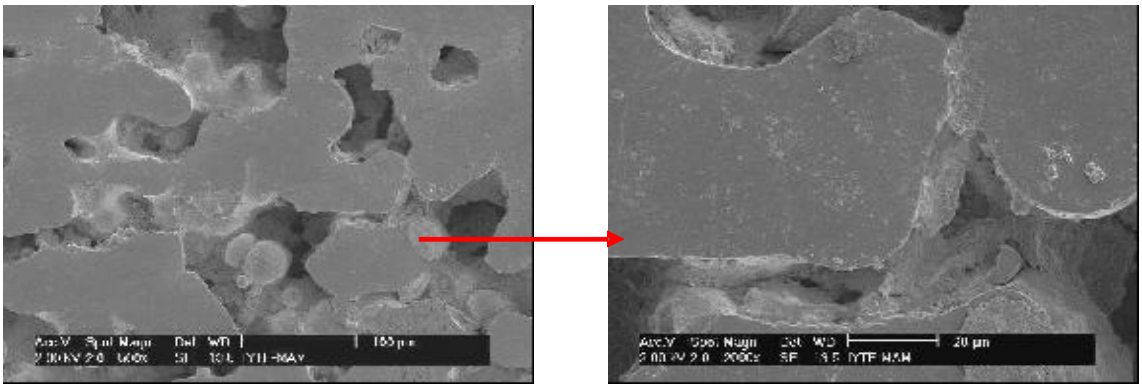

Figure 6.23. SEM micrograph showing the cross section of the porous plastics after loading at the stress level of 19 MPa.

6.5. Effects of Emulsion Constituent Concentrations on the Fracture Toughness of Material

The fracture toughness (K_{Ic}) values of the materials were measured using the SENB test configuration and are tabulated for varying water-surfactant and monomer concentrations in Table 2. It was found that K_{Ic} values decrease by 64% as the concentration of water-surfactant is increased by 38%. In contrast, K_{Ic} values increases by 104% as the monomer concentration increased by 34%. The results indicate that K_{Ic} is increasing as the pore fraction is decreasing and cell walls are thickening. Fig. 6.24 shows the fracture surface SEM micrograph of the SENB specimens with 40 and 29 wt.% of water-surfactant, respectively. A high concentration of water-surfactant in the emulsion resulted in an increase of pore fraction and reduction of the thickness of the cell walls as can be seen in Fig.6.24 (a). For this case, fracture occurs over a relatively smaller area by the tear of thinner cell walls. There is no noticeable plastic deformation on the fracture surfaces. For lower concentration, as shown in Fig. 6.24 (b), the porosity is lower and thicker cell walls forms where the filler PMMA beads are completely

embedded into the monomer phase, dissolved in it and connected very strongly. Fracture occurs over a larger area and for the extension of the crack a higher surface energy is required. This may result in improved fracture toughness of the material with a higher K_{IC} values.

Table 2. Fracture toughness of materials produced with various water/surfactant and monomer concentrations.

	Wt. %	Fracture Toughness, K_{IC} (MPa $m^{1/2}$)
Water-Surfactant	29	0.376 ± 0.005
	33	0.219 ± 0.041
	35	0.187 ± 0.006
	37	0.180 ± 0.010
	40	0.134 ± 0.026
Monomer (MMA)	15.5	0.158 ± 0.006
	18.3	0.246 ± 0.017
	19.7	0.274 ± 0.016
	20.8	0.322 ± 0.016

On the other hand, an increase in MMA concentration results in a significant increase of the fracture toughness values due to the formation of a low fraction of pores and relatively thicker cell walls with higher strength. Fig. 6.25 shows the SEM fracture surfaces of SENB samples produced with monomer concentrations of 15.5 wt.% and 20.8 wt.%, respectively. Similarly, as the concentration of MMA is increased as in Fig. 6.25 (b), much thicker cell walls form and fracture occurs over a large area [43].

6.6. Residual Mechanical Properties of Porous Plastic Materials after Cyclic Loading

Structural durability of plastic porous materials that are used as a mold material and subjected to high pressure cycles is important. To measure the residual mechanical properties and investigate the deformation mechanisms, cyclic loading experiments were conducted under compression mode at the maximum load level of 50, 62.5 and 75

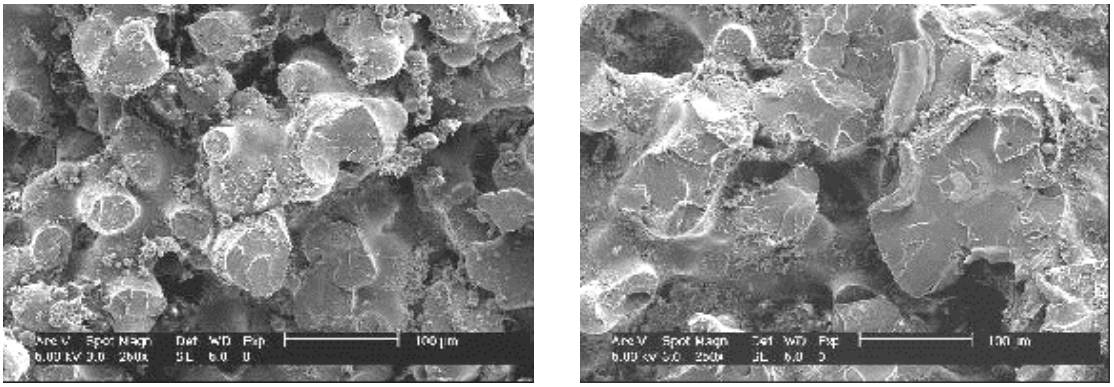

(a) (b)

Figure 6.24. SEM fracture surface micrograph of the SENB specimens with the water-surfactant concentrations of a) 40 and b) 29 wt.% (w/s=1/3).

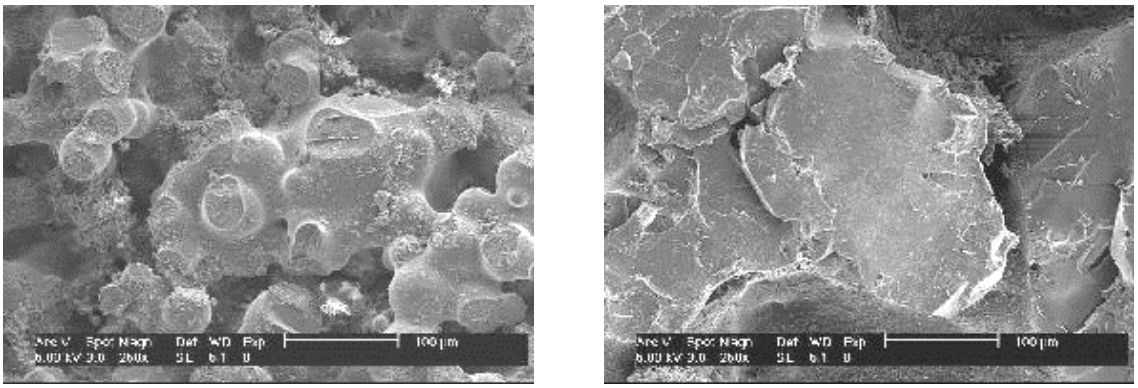

(a) (b)

Figure 6.25. Fracture surface SEM micrograph of the SENB specimens with the monomer concentrations of a) 15.5 and b) 20.8 wt.%.

of the collapse stress. The cyclic loading was performed for 1000 cycles, and then the specimens were subjected to static compression testing to measure the residual strength and modulus of the material. Fig.6.26 shows the comparison of compressive stress strain responses of the original specimen without cyclic loading and the specimens loaded at various stress level for 1000 cycles. The results show that the modulus of the specimen increases by about 52% as compared to un-cycled specimen. This may be associated with the fatigue of the cell walls and crack initiation and collapse of some cells during the repeated loading. Due to the collapse of the structure, modulus values may be increased while the strength is reduced due to the crack formation. Also the collapse strength values are very close to each other for cycled specimens and it is lower than the un-cycled one.

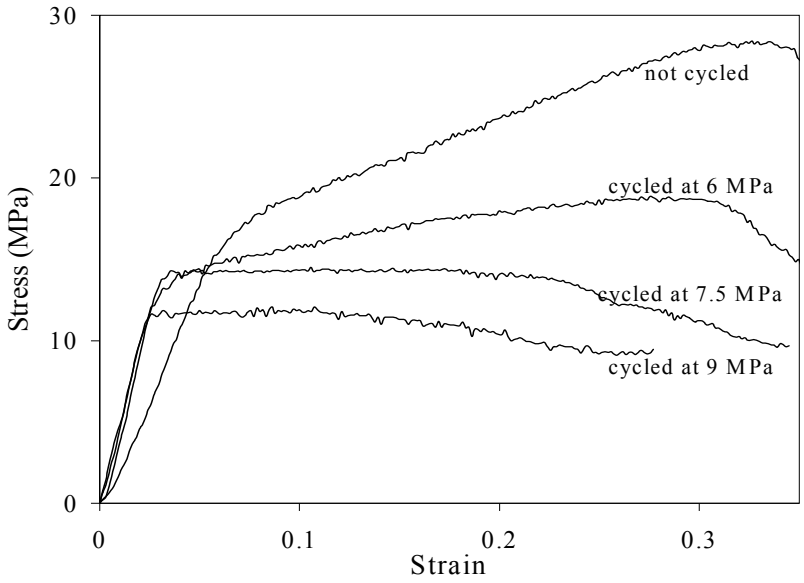

Figure 6.26. Compressive stress-strain responses of materials after 1000 cycle loading under the stress values of 6, 7.5, 9 MPa.

Chapter 7
CONCLUSION

PMMA-based open-cell porous materials were produced using various concentrations of water-in-oil emulsion liquid constituents and PMMA bead sizes. It was revealed that the porous network is mainly formed by the water droplets surrounded with surfactants and the cell walls are formed by the polymerized monomer molecules with the contribution of PMMA beads. To produce an optimized open-cell porous structure, it is essential to obtain homogeneous distribution of the water droplets with high connection and the stabilization of the emulsion throughout the polymerization reaction. It was found that constituent concentrations significantly affect the porosity, pore morphology, water permeability, collapse stress and elastic modulus of the porous plastics [44]. Percentage of the porosity increased from 34 to 47%, the permeability constant of the specimens was increased from 2.1 to 4.3 darcy as the amount of water-surfactant increased from 29 to 40 wt.%, respectively. Increasing the monomer concentration has reverse effect on porosity and permeability. Percentage of porosity is decreasing where the permeability constant of the material is increasing. It was also found that porosity and permeability values increase as the average particle diameter of beads used from 22 to 130 μm.

Performed mechanical tests showed that the material exhibits the compressive behavior similar to elastic brittle foams. It was found that the collapse stress and elastic modulus decrease from 24 to 4.9 MPa and from 824 to 224 MPa, respectively, as the concentration of water-surfactant increases from 29 to 40 wt.%. Furthermore, densities of the tested materials change in the range of 0.85 to 0.762 g/cm^3 for the given concentration range. Increasing the monomer concentration was resulted in formation of thicker cell walls and improved mechanical properties with increasing collapse stress and modulus. For the increase of average bead diameters from 22 μm to 130 μm collapse stress and modulus values decrease.

Mechanical compressive test results of the materials were related with the structural properties of the materials such as relative density based on the predictions of Ashby-Gibson and Roberts-Garboczi. It was found that the experimental data obtained from the compressive testing correlates well with the predictions based on Roberts-Garboczi model for overlapping solid spheres.

SENB test results and fracture surface investigations show that the porous plastic PMMA based materials fracture in brittle manner. It was found that lower concentrations of water and higher concentrations of monomer result in thicker cell walls and fracture zone passes through larger area and for the extension of the crack higher surface energy is required. So this was resulted in improved fracture toughness of the material with higher K_{IC} values.

Residual strength of the specimens after cyclic loading was investigated and it was observed that after 1000 cyclic loading all the materials loaded at various stress levels over and under the collapse stress have permanent deformations. After cyclic loading, increase of elastic modulus values and decrease of collapse stress values were measured.

Addition of nano scale montmorillonite particles improves the mechanical properties of the plastic materials. The specimen produced with the addition of 1 wt. % of surface modified montmorillonite exhibited 90 and 50% increase of collapse stress and elastic modulus values, respectively.

In the future studies, addition of nanoscale clay particles to the emulsion system may be studied and optimum clay concentration may be determined. Also, homogeneity and stability of the emulsion is very critical for the structure and hence the performance of the material. So, further studies may be performed to investigate the stability of the emulsion throughout the polymerization. This is also related with the reaction time and reaction time can be adjusted by the initiator concentration. So, studies may be performed to investigate the effects of the initiator concentration and reaction time on the properties of the materials.

REFERENCES

1. V. Mazzanti., The Technology That has Renewed Low Pressure Casting, *Process Engineering*, DKG 2002; 79 (1-2): E11-12.
2. E.J. Pique, L.J.M.G. Dortmans, G. de With, Fictitious Crack Modeling of Polymethyl Methacrylate Porous Material, *Material Science and Enginering*, 2002, (A335) 217-227.
3. A. Dortmans, H. Fischer, R.G. Nelissen, Prediction and Improvement of The Lifetime of Polymer Pressure Casting Molds, *Process Engineering* DKG 2002; 79 (1-2) :E45-48.
4. A. Dortmans, L.F. Batenburg, T.P.M. Koster, R.G. Nelissen, H. Fischer, Nanocomposite Materials: From Lab-scale Experiments to Prototypes, *e-polymers*, (http://www.e-polymers.org) 2002; (10): 1-10.
5. L.J. Gibson, M.F. Ashby, Cellular Solids, 2nd ed. Cambridge University Press, Cambridge, UK, 1997.
6. A.P. Roberts, E.J. Garboczi, Computation of The Linear Elastic Properties of Random Porous Materials With a Wide Variety of Microstructure, *Proceeding of the Royal Society of London A,* 458, 1033-1054, 2002.
7. X. Huang, W.J. Brittain, Synthesis and Characterization of PMMA Nanocomposites by Suspension and Emulsion Polymerization, *Macromolecules*, 2001, 34, 3255-3260.
8. J. Teckoe, Synthetic Molds Go Mainstream, www.ceramicindustry.com
9. J.T. Jones, M.F. Berard, Ceramics Industrial Processing and Testing, Iowa State University Press, Ames, Iowa, 1993.
10. http://unit.aist.go.jp
11. T. Thompson, The Rheology of Ceramic Kaolin's, *International Ceramics*, Issue 1, 2000.
12. http://www.asianceramics.com
13. Princeton University: ChE346- Colloidal Consolidation
14. B. Leach, Slurry Solutions for Sanitaryware**,** www.ceramicindustry.com
15. www.garoll.it
16. United State Patent 5522717
17. British Patent number GB1458203
18. European Patent number EP0516224

19. F. Hoffman, K. Delbruch, Patent No.250 690, Germany, 1909.
20. W. Bauer, H. Lauth, Patent No.656 134, Darmstadt, 1931.
21. P.J. Dowding, B. Vincent, Suspension Polymerization to Form Polymer Beads, *Colloids and Surfaces A*, 161, 2000, 259-269.
22. D. Blobdeu, M. Bigan, P. Despres, Ultrasound Suspension Polymerization Method for Preparation of 2-Hydroxyethylmethacrylate Macroporous Copolymers, *Reactive and Functional Polymers*, Volume 27, Issue 3, 1995, 163-1*73*
23. T. Liu, C. Burger, B. Chu, Nanofabrication in Polymer Matrices, *Progress in Polymer Science*, 28, 2003, 5-26.
24. N.D. Kaushika, K. Sumathy, Solar Transparent Insulation Materials: a Review, *Renewable and Sustainable Energy Reviews*, 7 (2003) 317–351
25. A.M. Hayes, A. Wang, B.M. Dempsey, D.L. McDowell, Mechanics of Linear Cellular Alloys, *Mechanics of Materials,* 36 (2004) 691–713
26. C. Park, S.R. Nutt, Strain Rate Sensitivity and Defects in Steel Foam, *Materials Science and Engineering* A323 (2002) 358–366
27. Arcos D., Ragel C.V., Vallet-RegmH M. Bioactivity in Glass/PMMA Composites Used as Drug Delivery System, *Biomaterials* 22 (2001) 701}708.
28. B. Pascuala, M. Gurruchagaa, M.P. Ginebrab, F.J. Gilb, J.A. Planellb, I. Goni, Influence of The Modification of P/L Ratio on a New Formulation of Acrylic Bone cement, *Biomaterials* 20 (1999) 465-474
29. M.J. Silva, L.J. Gibson, The Effects of Non-Periodic Microstructure and Defects on the Compressive Strength of Two-Dimensional Cellular Solids, *International Journal of Mechanical Science*, 39 (1997) 549
30. A.P. Roberts, E.J. Garboczi, Elastic Moduli of Model Random Three Dimensional Closed Cell Cellular Solids, *Acta Materialia*, 49, 2001, 189-197.
31. W.E. Warren, A.M. Kraynik, Linear Elastic Behavior of a Low Density Kelvin Foam With Open Cells, *Journal of Applied Mechanics*, 64, 787-794.
32. L.J. Gibson, M.F. Ashby, *Proceeding of the Royal Society of London A,* 1982, 383, 43.
33. A.P. Roberts, E.J. Garboczi, Elastic Properties of Model Random Three Dimensional Open-Cell Solids, *Journal of the Mechanics and Physics of Solids*, 2002, 33-55.

34. T.G. Nieh, J.H. Kinney, J. Wadsworth, A.J.C. Ladd, Morphology and Elastic Properties of Aluminum Foams Produced by a Casting Technique, *Scripta Materialia*, 38(10), 1487-1494, 1998.
35. M.W.D. Van der Burg, V. Shulmeister, E. Van der Geissen, R. Marissen, On the Linear Elastic Properties of Regular and Random Open-Cell Foams Models, *Journal of Cellular Plastics*, 33, 31-54, 1997.
36. S. Torquato, L.V. Gibiansky, M.J. Silva, L.J. Gibson, Effective Mechanical and Transport Properties of Cellular Solids, *International Journal of Mechanical Science*, 40, (1998), 71-82.
37. E.P. Giannelis, R. Krishnamoorti, E. Manias, Polymer-Silicate Nanocomposites: Model Systems for Confined Polymers and Polymer Brushes, *Advances in Polymer Science*, 138, 1999, 108-147.
38. R.J. Stokes, D.F. Evans, Fundamentals of Interfacial Engineering, Wiley-VCH, New York, USA, 1997.
39. Standard Test Methods for Plane-Strain Fracture Toughness and Strain Energy Release Rate of Plastic Materials, *American Society for Testing and Materials* (ASTM) D5045-91a.
40. T.L. Anderson, Fracture mechanics; Fundamentals and Application, 2nd ed. CRC Press, New York, USA, 1995.
41. K.Y.G. McCullough, N.A. Fleck, M.F. Ashby, Uniaxial Stress-Strain Behaviour of Aluminium Alloy Foams, *Acta Materialia*, 47 (1999) 8, 2323-2330.
42. C. Park, S.R. Nutt, Anisotropy and Strain Localization in Steel Foam, *Material Science and Engineering A*, 299 (2001), 68-74.
43. Y. Ergün, C. Dirier, M. Yılmaz, C. Tokman, M. Tanoğlu, Microstructure-Performance Relation in PMMA-Based Open-Cell Porous Materials for High Pressure Ceramic Sanitaryware Casting, *Key Engineering Materials*, Vols 270-273.
44. Y. Ergün, C. Dirier, M. Tanoğlu, Polymethyl Methacrylate Based Open-Cell Porous Plastics for High-Pressure Ceramic Casting, *Material Science and Engineering*.